Optimisation of the DØ Online Calorimeter Calibration for Run II

R. Chiche, C. de La Taille, Y Jacquier,
G. Martin, P. Pétroff, M. Ridel

Laboratoire de l'Accélérateur Linéaire
91898 Orsay France

October 17, 2001

D0 note 3914

Abstract

A complete simulation of the calibration signal and physics signal shapes has been performed. A method to correct the variation of the physics signal with an accuracy better than 1% in the whole calorimeter regions is proposed.

Contents

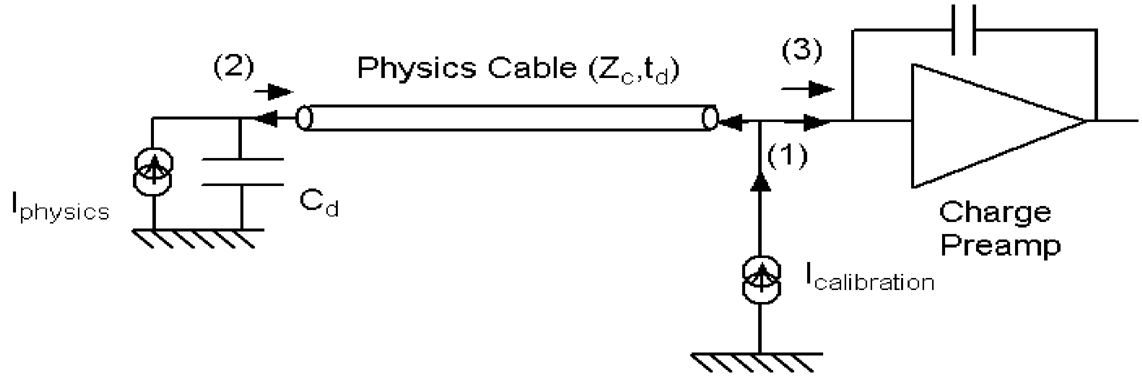

Figure 1: *Physics and Calibration Signals ways. The calibration signal is split in two parts.*

1 Introduction

The calorimeter online calibration consists in injecting of a reference signal at the preamplifier input, on the warm part of the signal cable instead of at the electrodes input. The advantage is the reduction of the number of cables going through the cryostat and accessibility to the calibration electronics. The drawback is the different paths followed by the physics signal and the calibration signal. Indeed, a first part of the calibration pulse goes directly into the preamplifier while a second one, after travelling through the signal cable, is partially reflected by the cell capacitance, C_d, and then reaches the preamplifier (see figure 1).

In this case, it is not possible to generate a calibration signal which accurately mimics the physics signal. Moreover due to the reflection, the calibration signal is more sensitive than the physics signal to the cable length and the cell capacitance variations. The figure 2 illustrates this difference at the preamplifier input.

As it is not possible to simulate exactly the physics signal using the calibration signal, a sufficient condition is that the calibration signal exhibits the same behavior than the physics signal with respect to parameters fluctuations. The main parameters affecting differently calibration and physics signals are: t_d (signal cable delay), Z_c (cable impedance), C_d (detector capacitance) and Z_{in} (preamplifiers input impedance). Among these parameters, Z_{in} is the worst known. It can vary from one preamplifier to another and also drift with time. The other parameters are stable in time but may vary from one channel to another.

In reality, the behavior of the calibration signal is not the same than the physics signal for a given parameters variation. This note describes the method used to extract the stable parameters quoted above and to simulate in a very realistic way both calibration and physics signals at a fixed preamplifier input impedance Z_{in}.

The stable parameters being determined for each calorimeter channel, a very simple correlation between the variation of Z_{in} and the variation of the calibration signal is computed. In the end, it is posible to compute the variation of the physics signal from a known variation of Z_{in}.

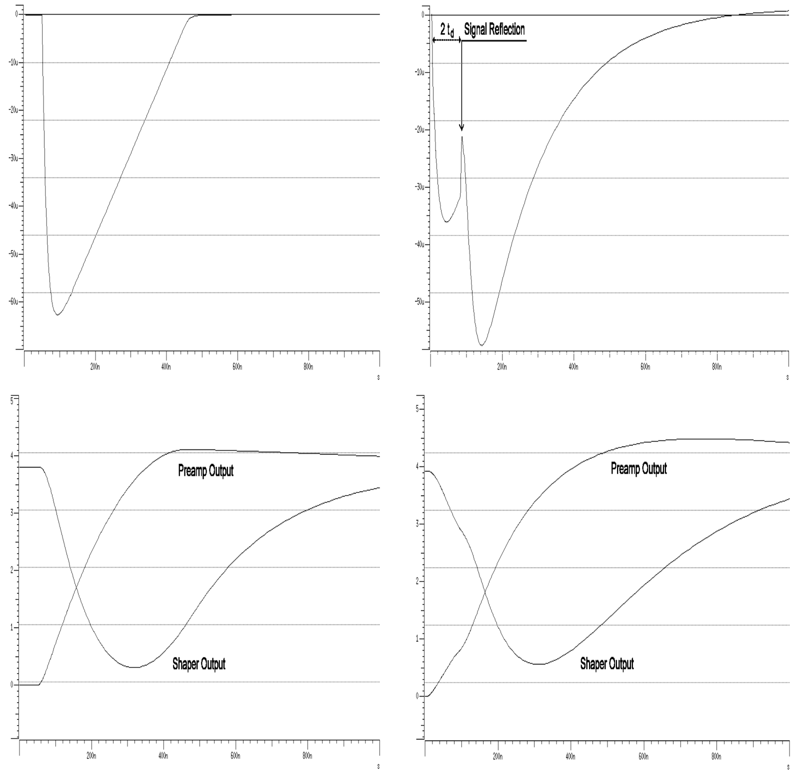

Figure 2: *Top: Physics signal and Calibration signal which shows the reflection of the pulse. Bottom: Physics and Calibration preamp and shaper output*

2 Description of the calibration setup

The calibration signal is shaped by an integration and a derivation of a step current signal as shown in fig 3. A brief description of the optimization of the calibration hardware components is given below (a more detailed description will be given in [1]).

The calibration system is divided in two parts. A specific pulser [1] sends a DC current and differential ECL commands to a fanout [2] which distributes the calibration pulse to the preamplifiers motherboards. On each fanout, there are switches receiving the DC current and the commands. The switches shape a calibration signal which is injected to the preamplifiers via the backplane of the motherboards (figure 4).

2.1 Description of the switches

The scheme of the calibration pulse generator is illustrated in figure 5. A DC current flows into a large inductance ($1mH$) through a normally on PMOS, as base of the NPN is low (0 V). A command signal (5 V) sets the NPN in saturation which turns the PMOS off. The inductor restitutes the current into the load (R_1, C_1, ..) producing a signal shape as shown in figure 3. Then this signal is injected with a impedance of $20K$ or $10K$ (depending of the preamplifier gain) in each preamplifier. Each calibration signal sees 6 preamplifiers.

[1] designed and constructed by LPNHE Paris
[2] designed and constructed by LAL Orsay

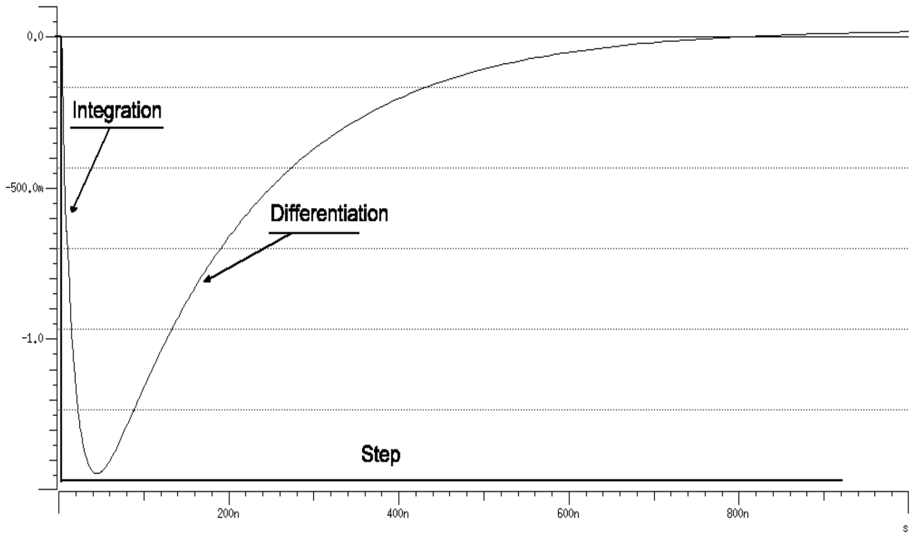

Figure 3: *calibration signal shaped by an integration and a derivation of a step current signal*

Species	A	B	C	D	E	F	G
physics signal peak in time (ns)	267	265	271	265	268	268	270
calib. signal peak in time (ns)	310	321	337	343	315	318	331

Table 1: Peak in time of physics and calibration signals for different preamp. type. Results are obtained with a constant cable length ($40ns$).

2.2 Effect of pole-zero compensation

Each calorimeter cell can be represented as a current source (physics signal) in parallel with a detector cell capacitance C_d which varies across the detector due to its geometry. The physic signal exhibits a pole $Z_{in}C_d$ due to the parallel combinaison of Z_{in} and C_d. This pole is then different for the various calorimeter regions (electromagnetic and hadronic regions).

The DØ calorimeter has 14 different cell capacitances as shown in table 2 and they are read out by 14 different preamplifiers types on which a pole-zero compensation is performed in order to compensate the $Z_{in}C_d$ pole effects on the physics signal. This technics allows to get the same signal shape at the preamplifier output and therefore to have the same downstream electronics (shapers ...).

The basic difficulty for the calibration is that the calibration signal is not previously shaped by a $Z_{in}C_d$ pole for the non reflected part. It can be expected that this bad behaviour will be mostly sensitive for preamplifiers corresponding to high capacitance values, namely for capacitance values corresponding to the hadronic part of the calorimeter as shown in figures 6 and 7. Variations in the peak in time value for the physics and for the calibration signals are given in table 1 for the same test stand that means with a constant cable length for each preamp. type.

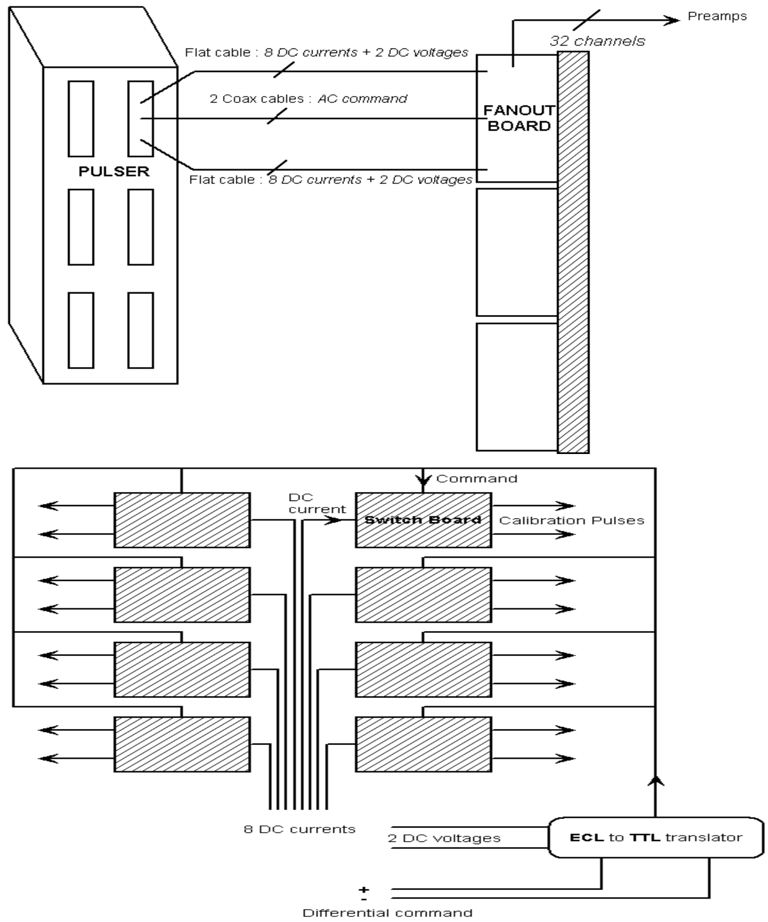

Figure 4: *Top: General layout from the pulser to the fanout. Bottom: Layout of the fanout to the Backplane of the preamp boxes*

Species	A	B	C	D	E	F	G
C_d(pF)	416	1265	2182	4028	403	881	1458
Species	Ha	Hb	Hc	Hd	He	Hf	Hg
C_d(pF)	1974	2296	2597	2837	3185	3604	4088

Table 2: Preamp species A, B, C, D are high gain with a feedback capa of 5pF the other species are low gain with a feeback capa of 10pF

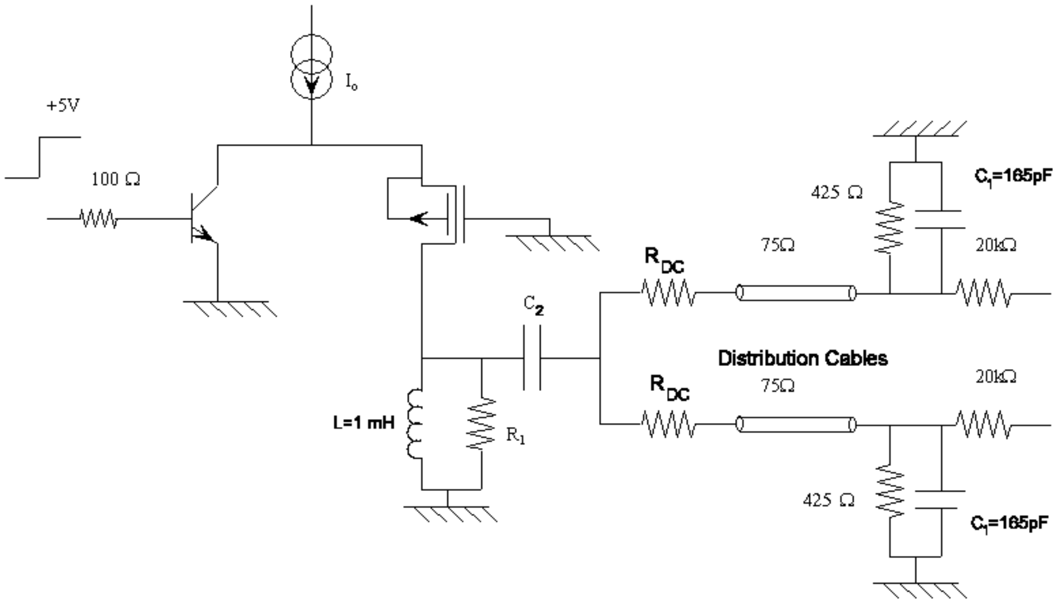

Figure 5: *drawing of the calibration switch*

3 Measurement of the stable parameters

The first step of a realistic simulation requires to measure precisely the stable parameters which shapes both the calibration signal and the physics signal at each calorimeter channel.

3.1 Time Domain Reflectometry (TDR)

For this purpose, a card has been designed and built at LAL Orsay. It is plugged in place of a preamplifier motherboard and allows to measure successively 48 channels by reflectometry method. A step signal is injected at the input of the preamplifier which is replaced by a well known 30Ω impedance. This signal follows exactly the path of the calibration signal. The result of the reflection of the signal on the cell capacitance is measured and registered at the input of the cable.

The theoretical output signal obtained for a step at the input for a lossless cable is shown in figure 8. The amplitude of the output step gives the cable impedance, Z_c, the length of the ouput step gives two times the cable delay and the following exponentiel gives the cell capacitance. After theses measurements, Z_{in} remains the only unknown parameter and also the only one evolving in time.

3.2 Measurements in a test stand

In order to check the accuracy obtainable, measurements have been performed on a test stand (figure 9) where the step signal goes through a DØ type calorimeter cable with a known capacitance at the end. The cable length and impedance can be easily extracted from the output signal but it is more difficult to extract the capacitance. Low capacitance values are badly extracted but values higher than 400 pF are estimated within an accuracy

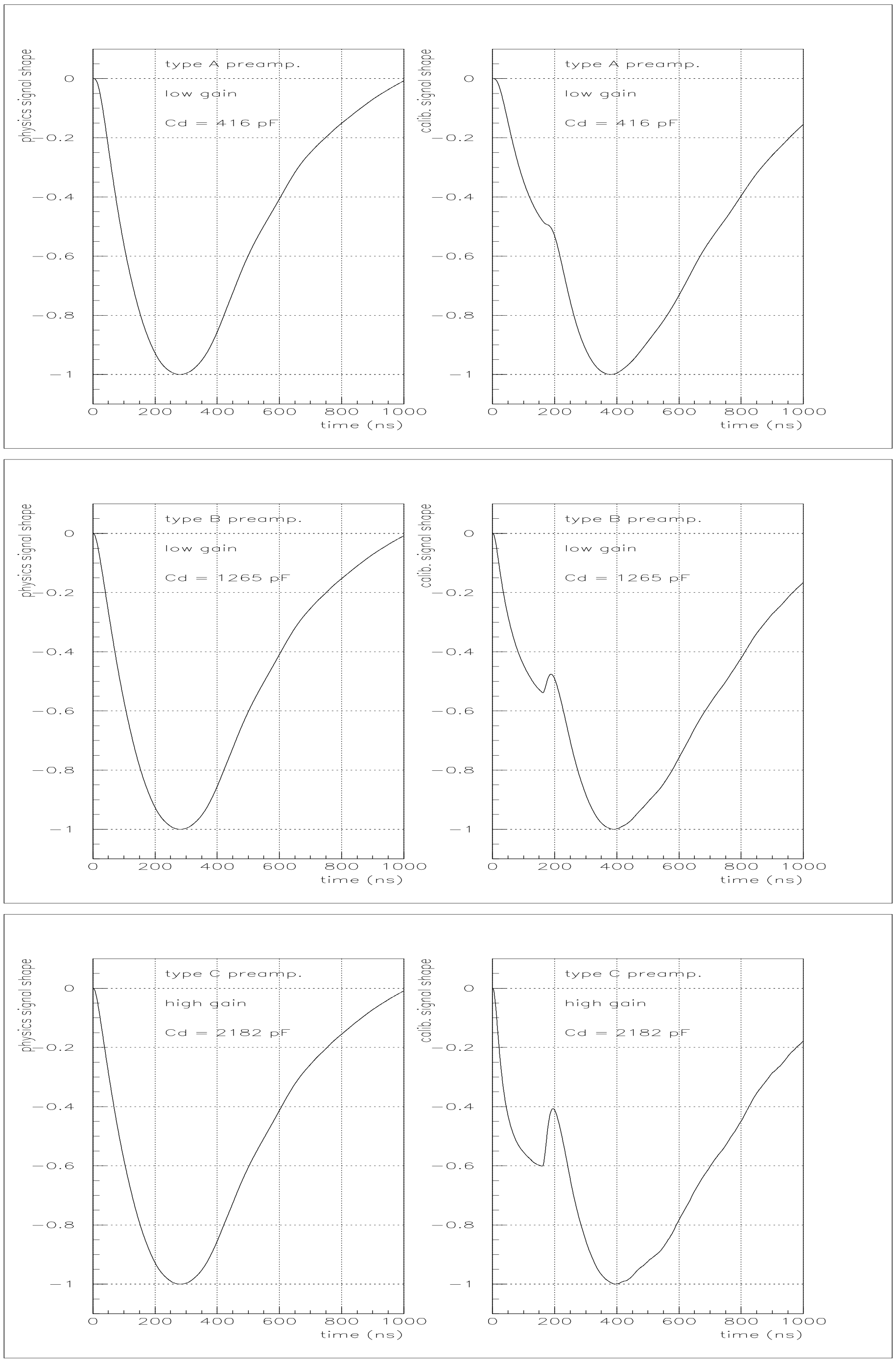

Figure 6: *Physics signal and Calibration signal preamp A, B and C*

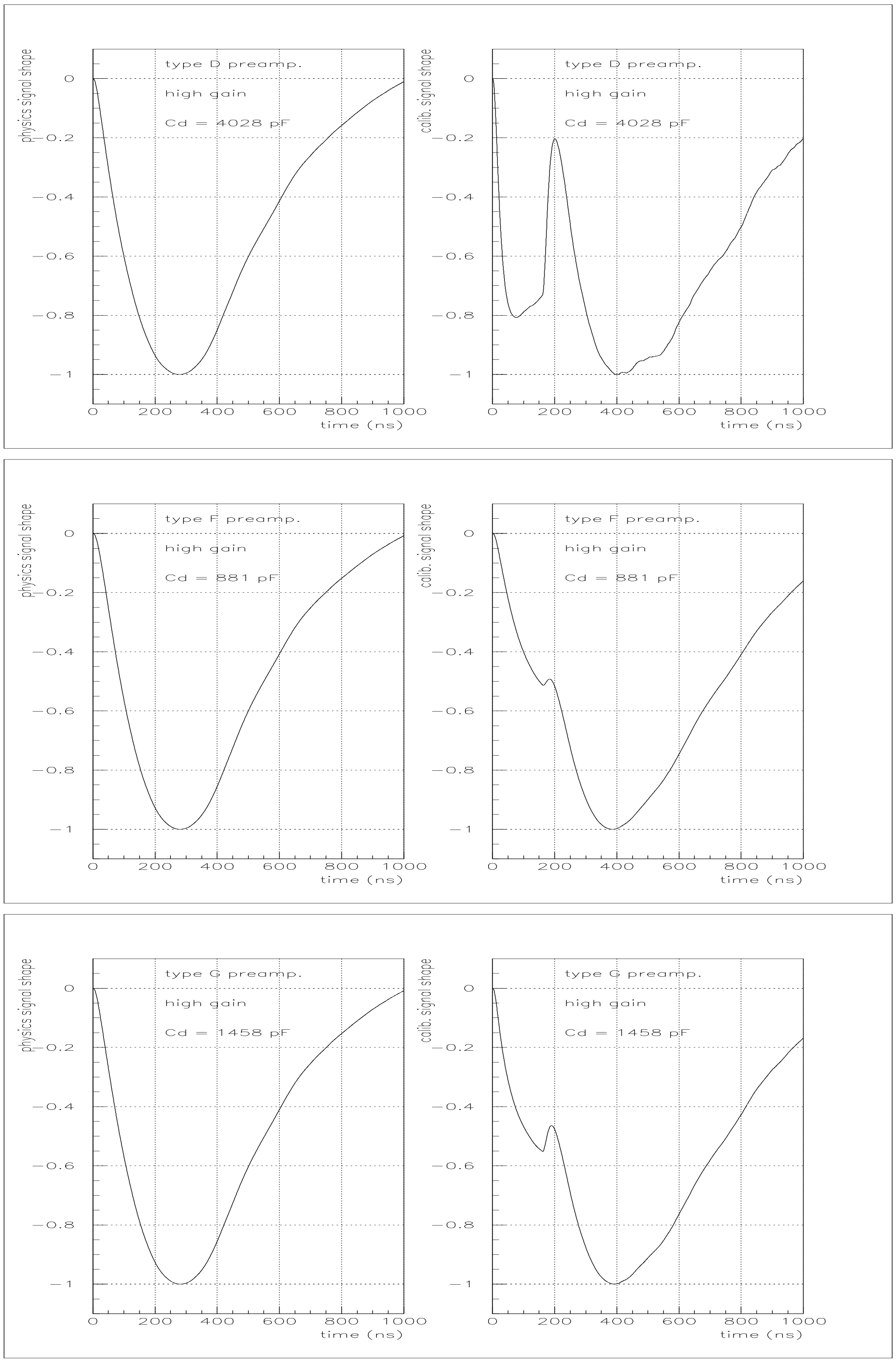

Figure 7: *Physics signal and Calibration signal preamp D, F and G*

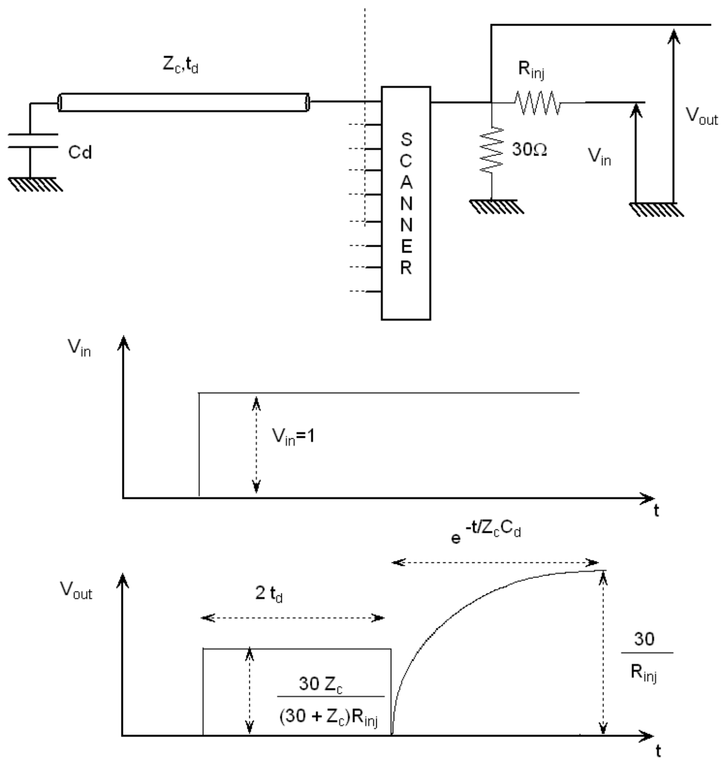

Figure 8: *Theoretical signal for a lossless cable expected with the TDR measurement.*

of 2 to 3% (as shown in table 3). For memory the range of the cell capacitances of the calorimeter is going from 400 pF to 4 nF.

Already at the level of a test stand, we see that it will be difficult to reach a good accuracy in the cell capacitance measurement for small values of C_d. But as stressed previously, the main point is the relative dependance of the calibration signal versus the physics signal in function of the cell capacitance itself.

3.3 Measurements of calorimeter parameters

The results of the measurements performed on the DØ calorimeter channels are shown in figure 10. This figure shows the result for three different species of preamplifiers corresponding to three different values of cell capacitances (400 pF, 1000 pF and 4000 pF). The signal shape looks more complicated than the one observed in the test stand.

The figure has been divided in five zones. The zone number increases from the left to the right corresponding to the propagation of the signal from the preamplifiers to the calorimeter cells. The zone 1 corresponds to the cable length L_2 between the preamplifiers box and the feedthrough. The step is not flat due to parasitics in the card itself. The bump in zone 2 is due to the inductance of the feedthrough itself. The zone 3 corresponds to the cable length L_1 between the feedthrough and the strips of a printed circuit connecting the cells. The bump in zone 4 is due to the inductance of these strips. The strip length depends on the cell position in a calorimeter module. Finally, the zone 5 corresponds to the cell capacitance.

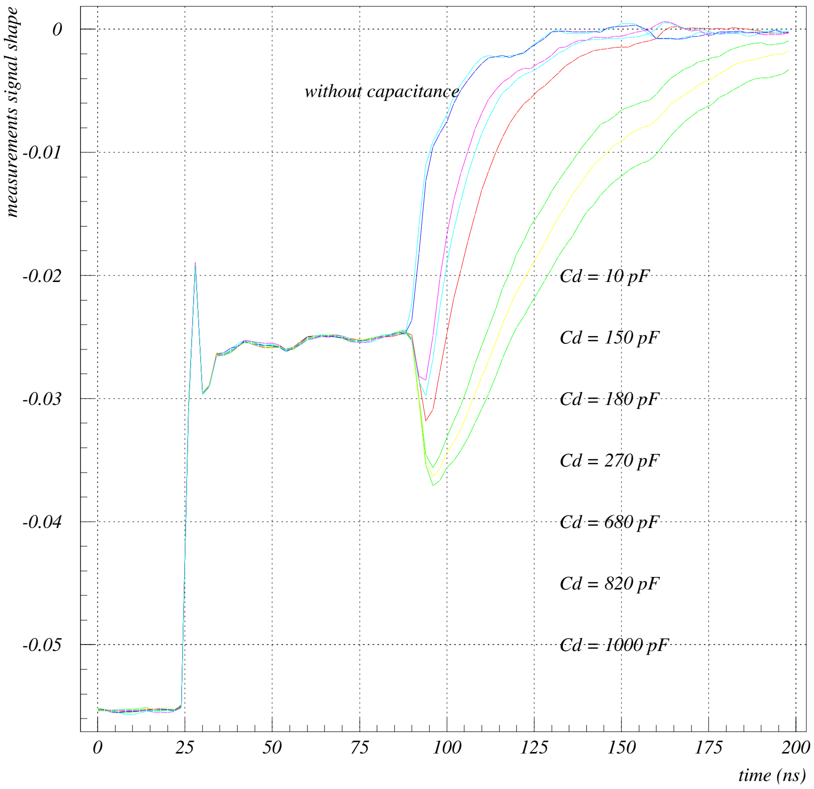

Figure 9: *Measurements in a test stand with well know capacitance values*

As a conclusion, it turns out that the diagramm shown in figure 8 represents a too naive model to fit the data. A more complicated but more realistic model is necessary to understand the 5 zones dividing the signal.

3.4 A more realistic model

A more realistic model obviously needs more parameters. This model is presented in figure 11. It takes into account the feedthrough (inductance L_f) and the strip which lies between cable and electrode (inductance L_s and capacitance C_s). The cable is divided in 2 parts: one before the feedthrough (R_2,L_2) and another after (R_1,L_1). Then comes the capacitance of the detector cell, C_d. There are now eight stable parameters to be extracted from the measurements. We will see in the following that a 9^{th} parameter which reflects the skin effect in the cables has to be taken into account and estimated.

3.5 Extraction technics for the stable parameters

The zone 5 which could naively corresponds to the cell capacitance effect only, depends in fact on other parameters like the strips capacitance and inductance and the skin effect in the cables. The fit itself will be unable to disentangle these parameters and we can

capacitance value (pF)	fitted value (pF)
0	10.92
10	17.65
150	154.1
180	190.1
270	288
680	688.8
820	835
1000	1007

Table 3: values of the true capacitances and the measured one

predict that the capacitance value deduced from the fit will not correspond to the true value.

The determination of the parameters is done in two steps. First the impedance and the length of the cables are deduced from a fit of corresponding regions of the step response as shown in figure 12. Second, the strip impedance and capacitance and the cell capacitance are calculated from a fit with a theoretical model (see appendix 1) illustrated by the diagram of the figure 11. In order to decouple the variables, the fit itself is performed first in the region where the strips inductance has an effect (zone 4) then fixing this parameter a second fit is performed to determine the strip capacitance and the cell capacitance (both are in parallel and cannot be disentangled by the fit). Finally, the skin effect is fitted on the measurement of a non connected cable (no cable after the feedtrough), the impedance and the length being extracted previously (see figure 13). The skin effect is assimilated to a delay T_s added to the propagation time in the cable. It has a fixed value depending on the cable characteristics. More details on the method can be found in appendix 1 and more precisely the transfer functions defined at each step of the signal propagation.

The final result on the simulation of a step signal ouput for a capacitance cell of 400 pF is shown in figure 14. The agreement with the data is fairly good and reproduces well the different features of the experimental response.

4 Simulations of the physics and calibration signals

It is mandatory to cross check the method of parameters extraction as the simulation of the physics signal requires the knowledge of these parameters. In the contrary, the calibration signal can be computed either from the convolution of the measured response to a step signal with the switch, preamp and shaper transfert functions either from the extracted parameters using a filtering technics and a convolution with the transfert functions of the switch, the preamp and the shaper.

The cross check is performed first on the reponse to a step signal. The comparison is done in fig 15 for a type E channel and in fig 17 for a type D channel. The full simulation is in good agreement with the measurements.

The second cross check is performed after convolution with the switch, the preamp and the shaper transfert functions. It is shown in fig 16 and fig 18 both for type E and type D channels. For recall type E has the lowest nominal capacitance ($403pF$: 3^{rd}electromagnetic floor), type D has the largest one ($4028pF$: hadronic floors). The

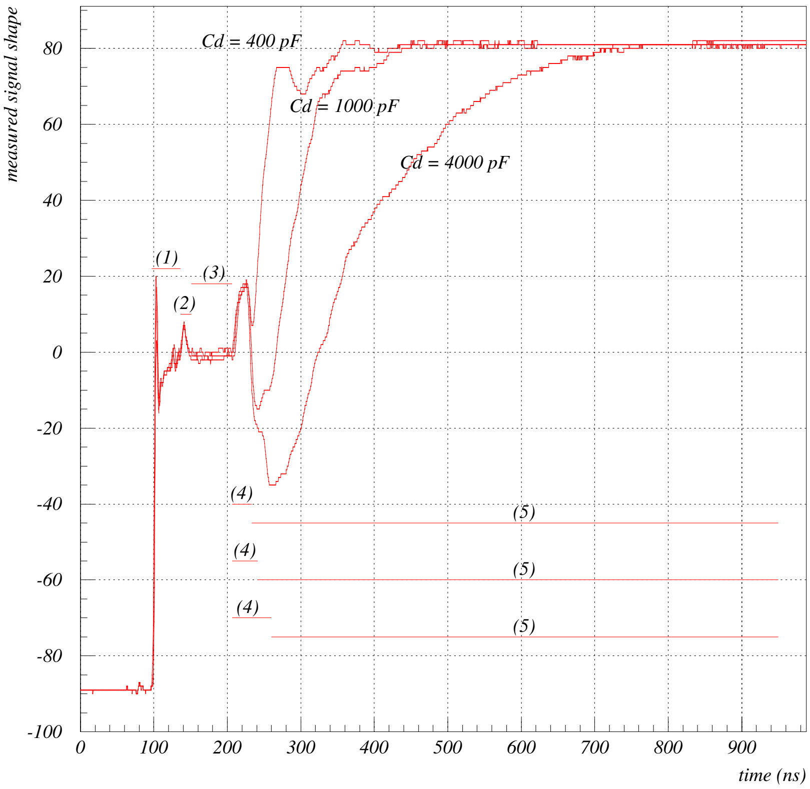

Figure 10: *Measurements of three different species of cell in the calorimeter. The zones are quoted from 1 to 5*

correspondance between preamplifier species and calorimeter layers is given in figure 19. The agreement is good at this level too.

Finally the full comparison is done between the full simulation of the calibration signal and the mesurements performed in situ on the calorimeter with the whole set of calibration system. It is shown in fig 22 for different type of channel. Types A, E and G simulation are in very good agreement with the data. The measurements in situ show some discrepancies with the simulation for type D channels, but the position of the maximum is well reproduced. Also one can notice that the simulation superimposed on the top of the measurements on figure 22 is the one using directly the reflectometry measurement then some convolutions (without parameter extraction). Z_{in} value is given by the reflectometry card itself (=30 Ωms) and can not be adapted to the measurement values. For type D channels, it explains the amplitude differences on the last part of the signal, this amplitude is driven by Z_{in}. The shape differences on the first part of the signal for type D preamp. is not understood for the moment.

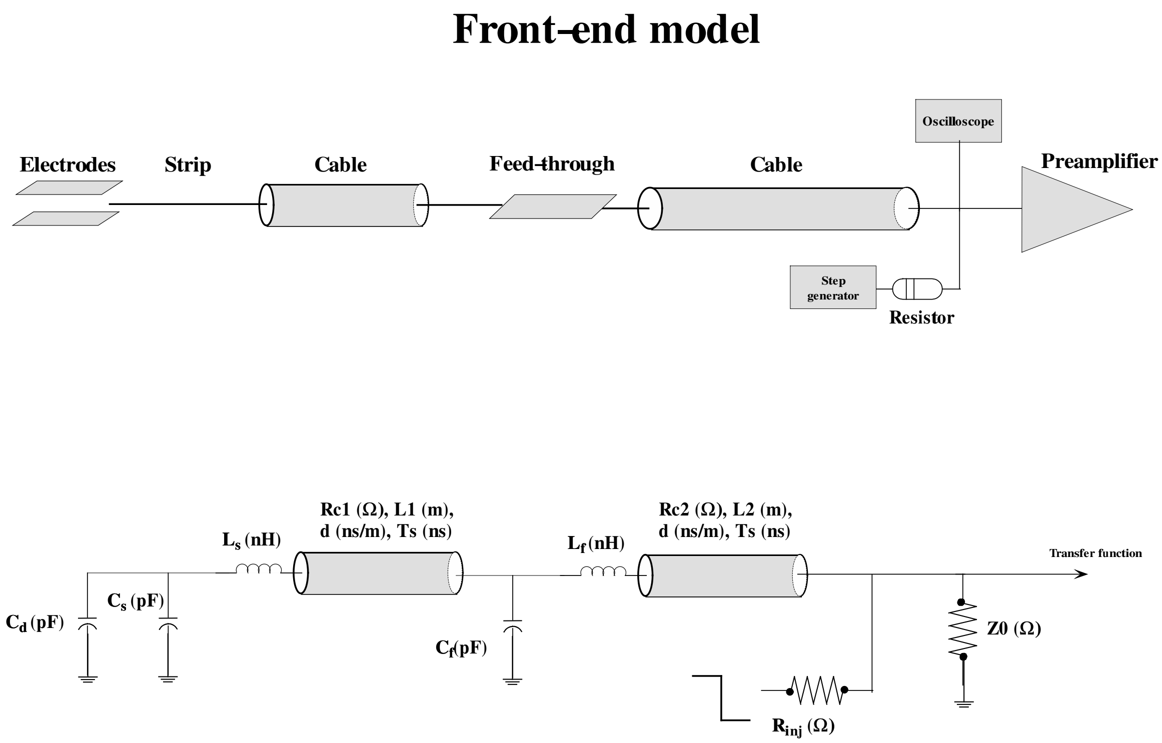

Figure 11: *Theoretical scheme used in the fit*

5 Calibration Method

As the 3^{rd} electromagnetic compartment is the most sensitive to the fluctuations of the electronics (shower maximum), we shall first study a calibration method on channels with type E preamplifiers which corresponds to the central region. A similar study has been performed in the endcap region with type F preamplifier.

The nine stable parameters of 521 type E channels have been determined. The normalized χ^2 resulting from the fit of R_{c1}, R_{c2}, L_s, and C_d is given in figure 23. A cut is applied on the χ^2 distribution which reduces the number of channels to 419.

The distribution of these last 4 parameters are shown in figure 25 after the χ^2 cut.

The cable lengths, L1 and L2, are directly deduced from the experimental step response. The result is shown in figure 24. The top view gives the distributiuon of the sum of the lengths with an RMS of 0.55 ns and a mean value of 56.3 ns (1%). In the following, in order to study the variation of the calibration and the physics signals with Z_{in}, the mean values of the stable parameters of 419 channels will be used.

5.1 Calibration and physics signals versus Z_{in}

The nine stable parameters being determined, the next step in this study is to evaluate the variation of the calibration and the physics signal in function of Z_{in}, the input impedance of the preamplifier. To perform this computation, the stable parameters mean values are fed into the full simulation.

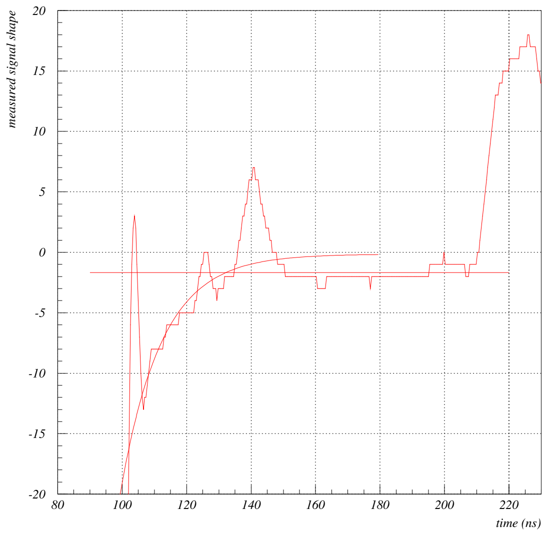

Figure 12: *impedance fits*

The simulation is performed first at a fixed Z_{in} value equal to 30Ω and the maximum value of the physics signal at t_{max} is taken as a reference. Z_{in} is varyed from -20% up to 20% by steps of 5%. At each Z_{in} value the physics signal is computed at t_{max} and compared to the reference point, the result is $\Delta phys^{t_{max}}$.

The variation of the calibration signal from the reference point can be estimated at any time which has to be optimized in order to get the best accurate correction on the physics signal variation. Figure 26 shows the distribution of $\frac{\Delta cal^t}{\Delta phys^{t_{max}}} - 1$ as a function of time. A very interesting point for the calibration could be the point A on the figure where $\frac{\Delta cal^t}{\Delta phys^{t_{max}}} - 1$ is equal to 0 which means that the variation of the calibration and the physics are the same. Unfortunately this point is on a steep slope and is not valid for negative variation of Z_{in}. The point B looks also interesting as it is a fixed point whatever the variation of Z_{in} is. But at this point$\frac{\Delta cal^t}{\Delta phys^{t_{max}}} - 1$ is very close to -1 that means that there is a very weak correlation between the variation of the calibration and the physics signals. The calibration method presented here allows to correct for Z_{in} variations. This is a difficult point its impact physics and calibration signals is different. Of course the electronic chain after preamplifiers may change also and it is needed to calibrate it. A change in the point B or fixed point value as it is independent of Z_{in} can indicate which part of Z_{in} or the rest of the chain should be calibrate. A variation of the chain can not be simulated here so all the results given in the following deal with Z_{in} calibration.

The point at t = 200 ns looks interesting as the absolute variation is at the maximum. At this point a linear fit reproduces the variation of Δcal versus ΔZ_{in} as shown in figure 27. Assuming that Z_{in} is not varying by more than 20% from its nominal value 30Ω, the error on ΔZ_{in} is at most 1.5% and the reflected error on the variation of the physics signal is 0.2% only.

The point at t = 345 ns looks interesting too as it corresponds to the maximum of the calibration signal at the reference point (Z_{in} = 30 Ω). At this point the amplitude is

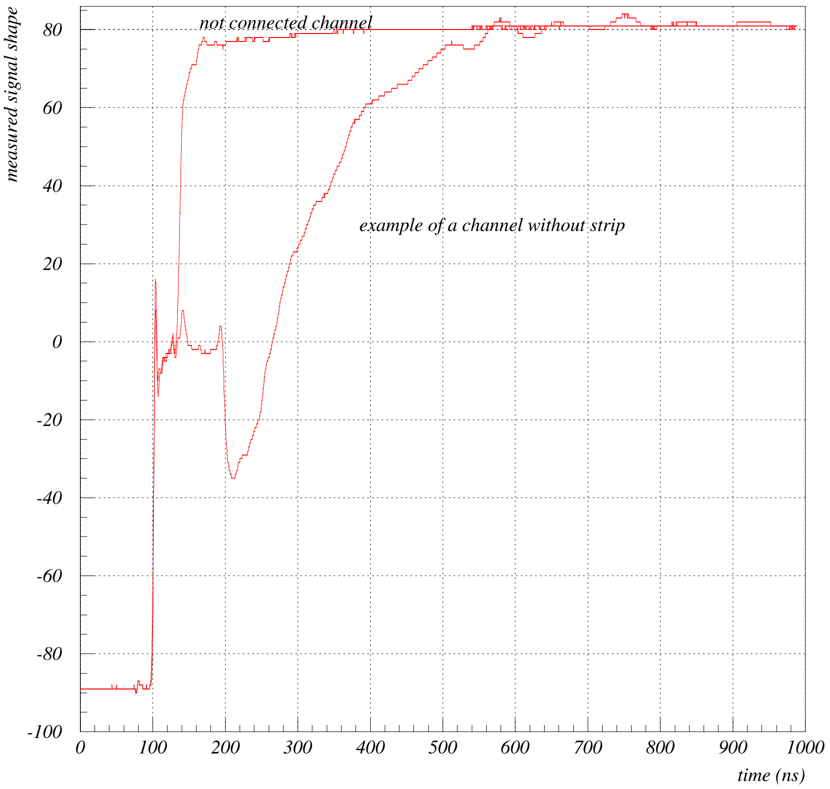

Figure 13: *how to get the end of the ouside cable*

varying slowly and we can expect that the measure of Δcal is more accurate. The results of a linear fit (top) and a polynomial fit (bottom) are presented in figure 28.

The linear fit induces an error on ΔZ_{in} of at most 1.5% but the polynomial fit improves the error to 0.4% resulting in a negligeable error on the variation of the physics signal. For recall, the stable parameters are assumed witout errors up to now.

A study has been performed on the effect of the distribution of the stable parameters. The results are shown in table 4. This table gives the errors on the calibration and on the physics variation assuming a $\pm$ one σ standard deviation in the distribution of R_{c1}, L_1, R_{c2}, L_2, L_s and C_d (figures 24 and 25).

If the simulation of the calibration and the physics signals is performed channel by channel the errors quoted above do not applies as we use the parameters values corresponding to one specified channel. It remains only the errors introduced by the fits to extract the stable parameters.

These errors are estimated from several measurements performed on one channel. The corresponding distributions are shown in figure 29. On this normalized distribution appear only the channels measured at least twice. The table 5 shows the number of time a defined channel has been measured. It also shows that some channels on the preamplifier motherboards are not measured due to some addressing problems on the reflectometry board.

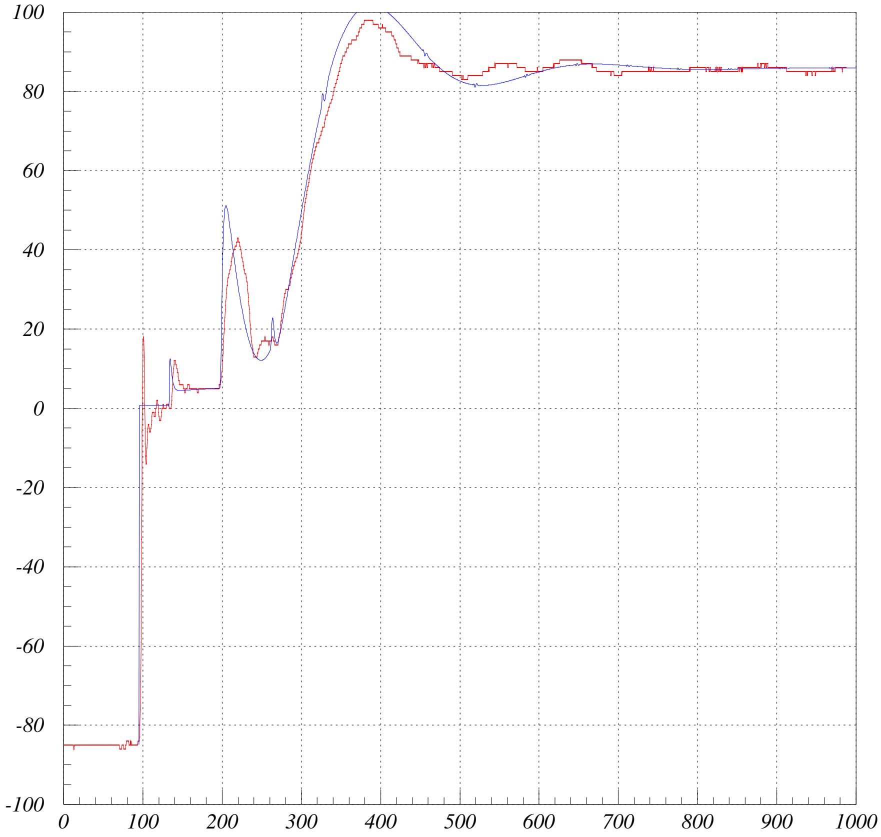

Figure 14: *Global Calibration Simulation*

$\pm\sigma$ on :	$\delta(\Delta_{cal}^{t=345ns})$	$\delta(\Delta_{phys}^{t=t_{max}})$
$L_1 + L_2$	0.08%	0.014%
R_{c1} or R_{c2}	0.18%	0.12%
L_s	0.004%	0.024%
C_d	0.1%	0.04%

Table 4: Contributions in the errors on the variation of the calibration and physics signals from $\pm\sigma$ variations in the stable parameters distribution

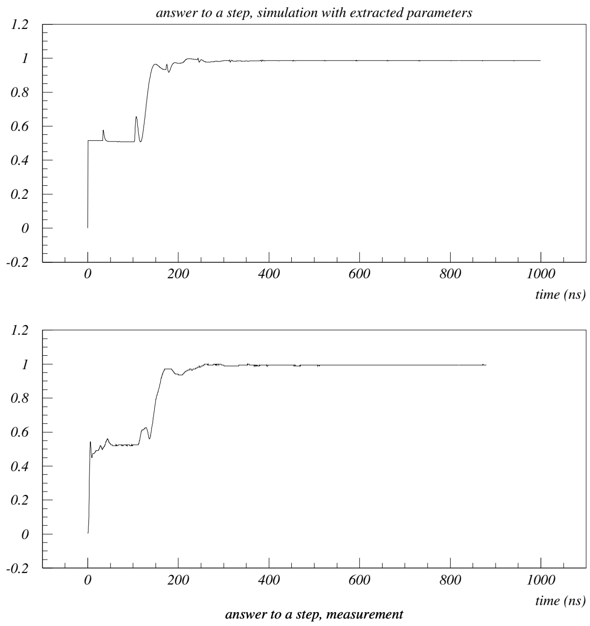

Figure 15: *simulated and measured answer to a step for a type E preamp.*

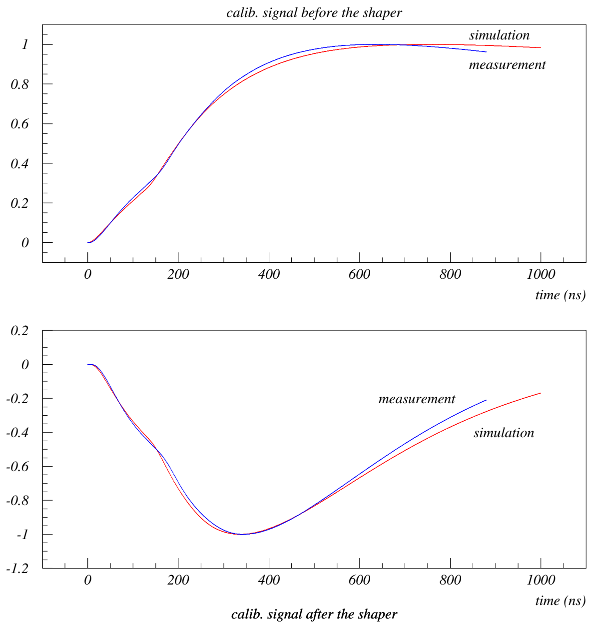

Figure 16: *simulated and measured calibration signals before and after the shaper for a type E preamp.*

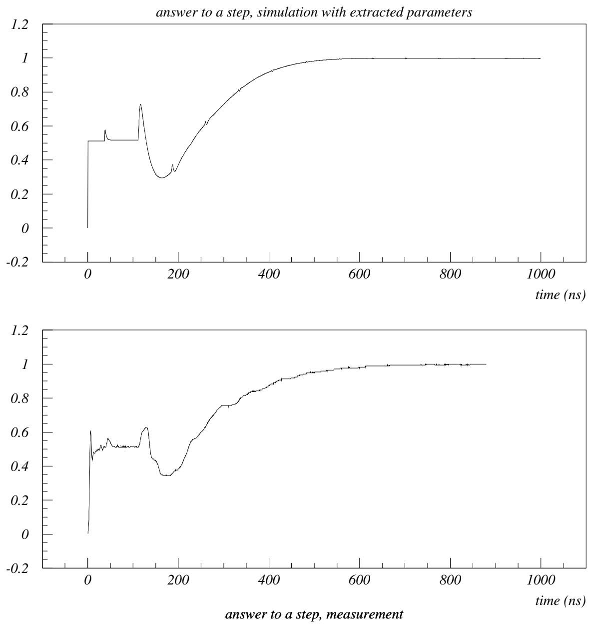

Figure 17: *simulated and measured answer to a step for a type D preamp. (4nF capacitance)*

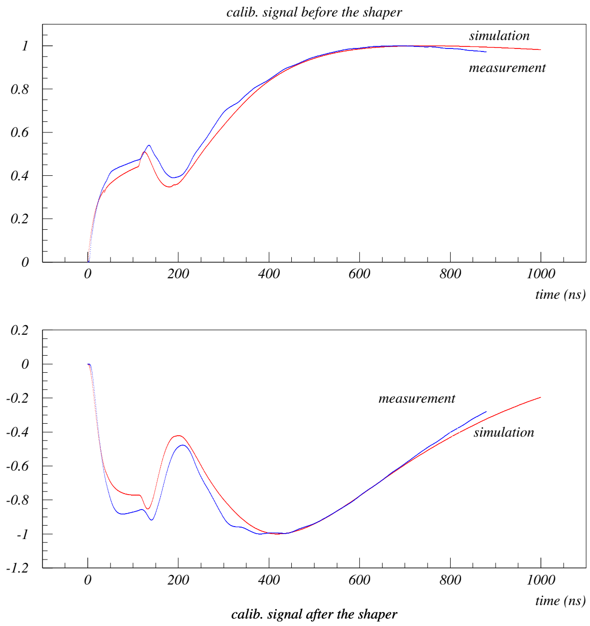

Figure 18: *simulated and measured calibration signals before and after the shaper for a type D preamp.*

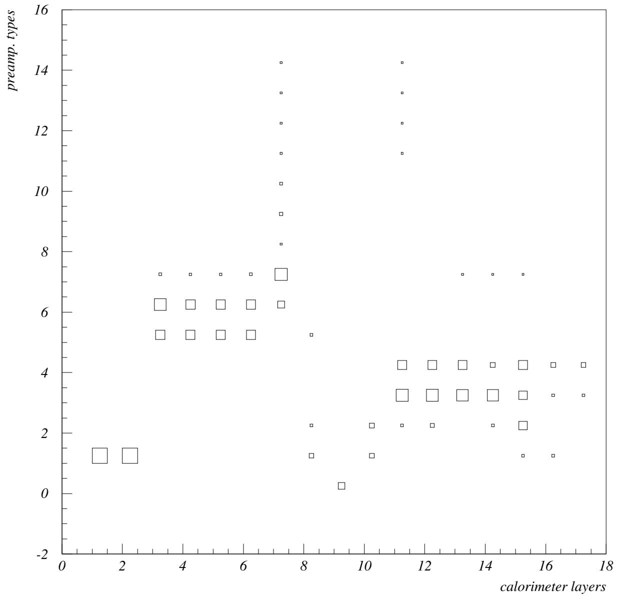

Figure 19: *maping of the preamp. types in the whole calorimeter*

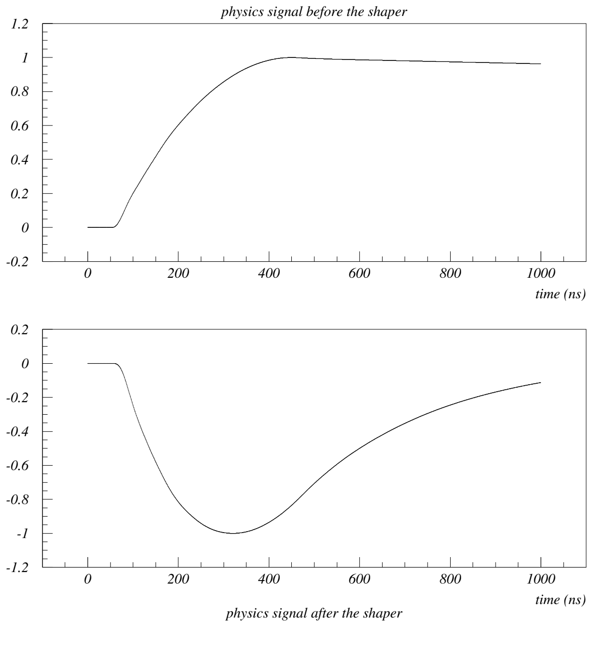

Figure 20: *simulated physics signal for a type E preamp.*

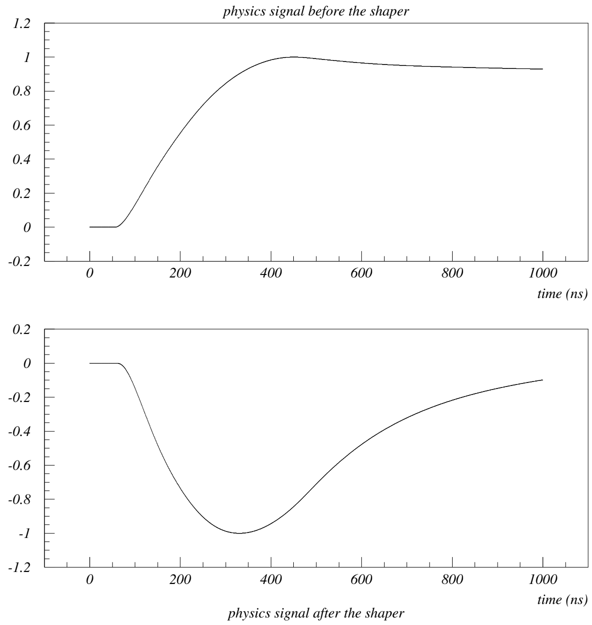

Figure 21: *simulated physics signal for a type D preamp.*

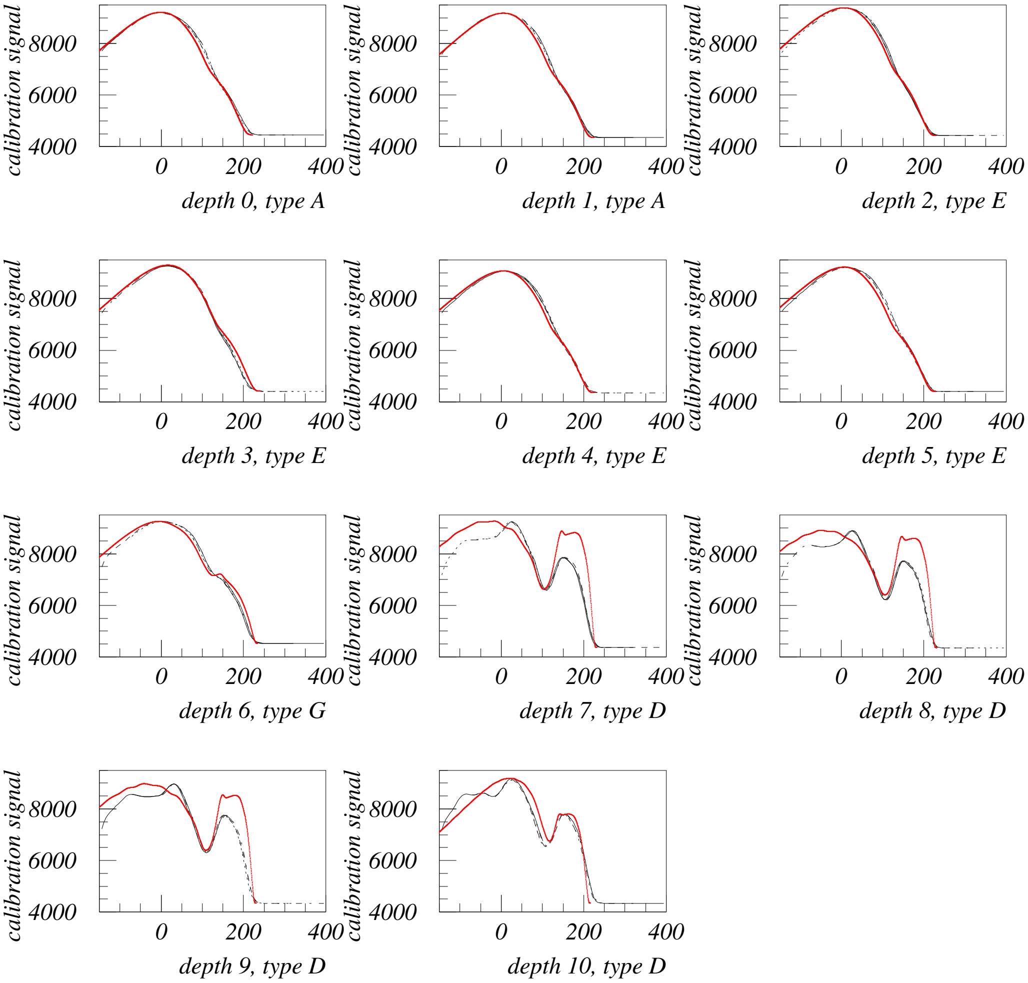

Figure 22: *Comparison between the Calibration Simulation and the measurements*

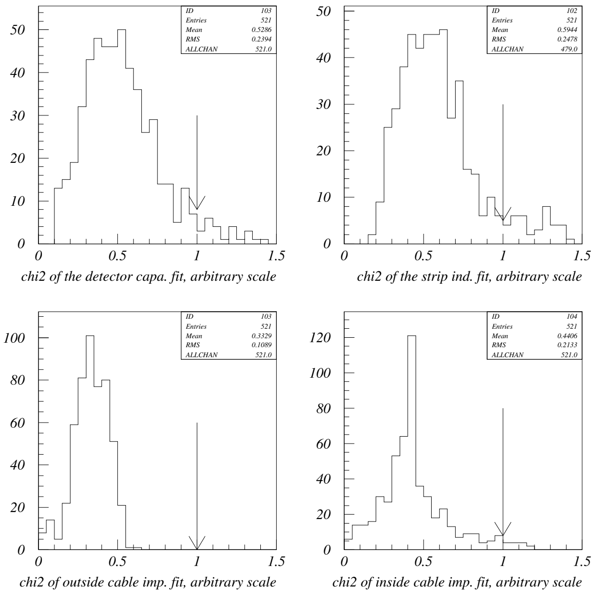

Figure 23: χ^2 *distribution (arbitrary scale) for the 4 fits performed in the extraction procedure. The arrows show where the quality cuts are applied.*

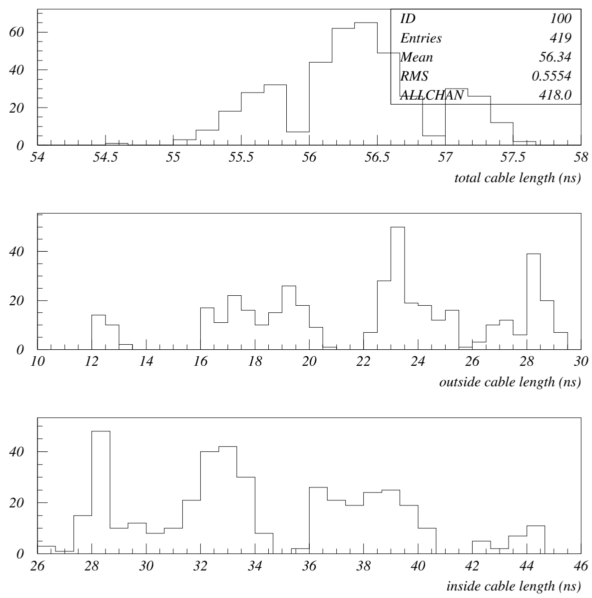

Figure 24: *cable length distributions for channels with type E preamp. (barrel)*

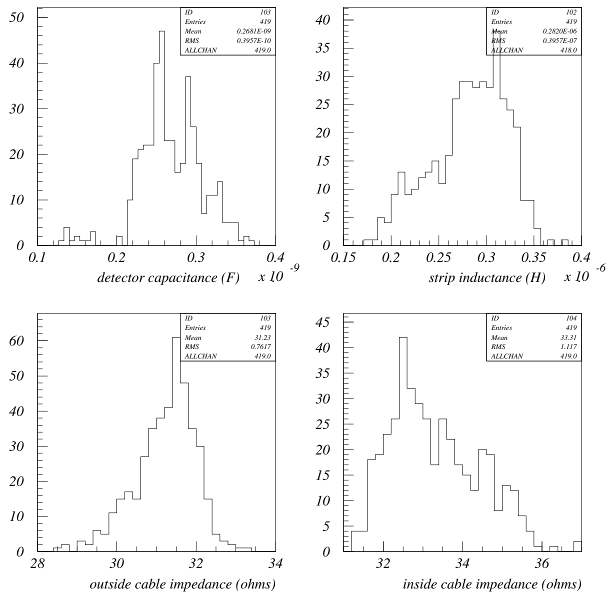

Figure 25: Rc_2, Rc_1, L_s *and* C_d *distributions for channels with type E preamp.*

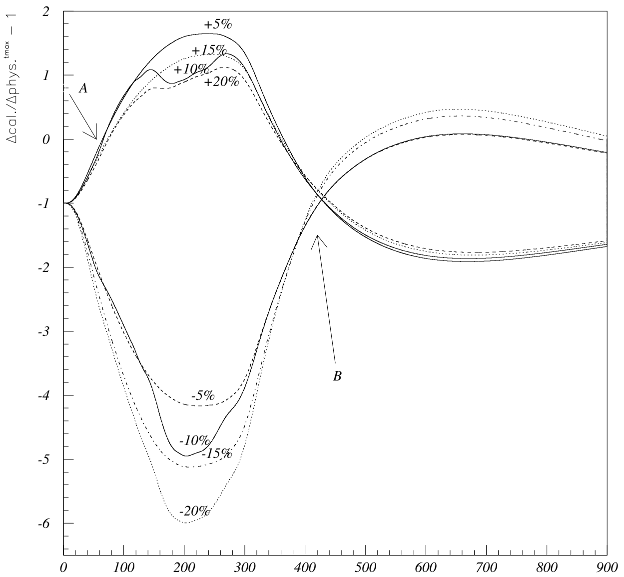

Figure 26: $\frac{\Delta cal^t}{\Delta phys^{tmax}} - 1$ *for a variation of* Z_{in} *of* $\pm 5\%$, $\pm 10\%$, $\pm 15\%$ *and* $\pm 20\%$

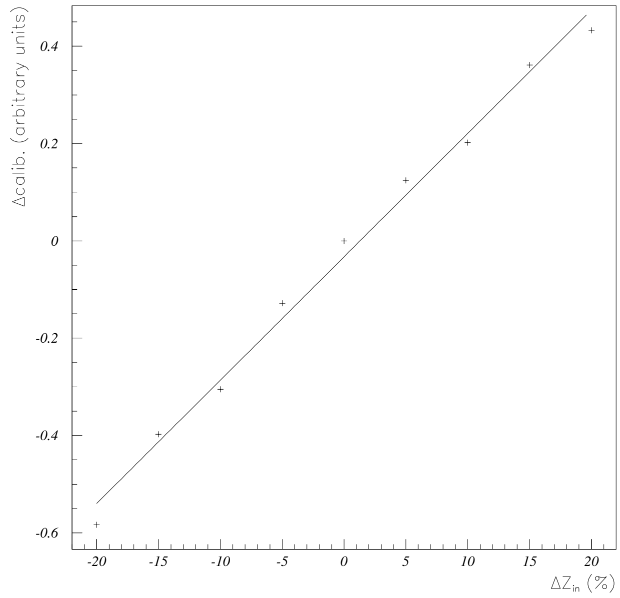

Figure 27: *linear fit results of* $\Delta cal(t = 200ns)$ *as a function of* $\Delta Z_{in}(in\%)$

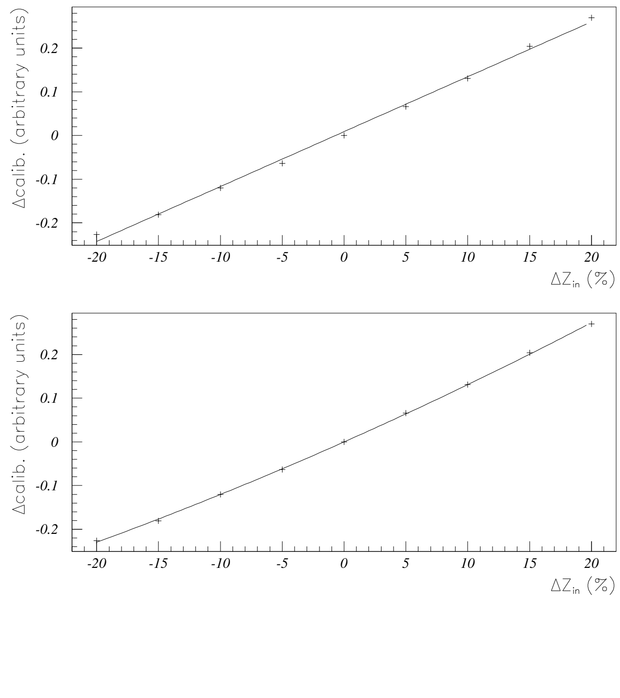

Figure 28: *linear fit (on top) and polynomial fit (on bottom) results of* $\Delta cal(t = 345.2ns$*, calibration peak in time for standard parameter set) as a function of* $\Delta Z_{in}(in\%)$

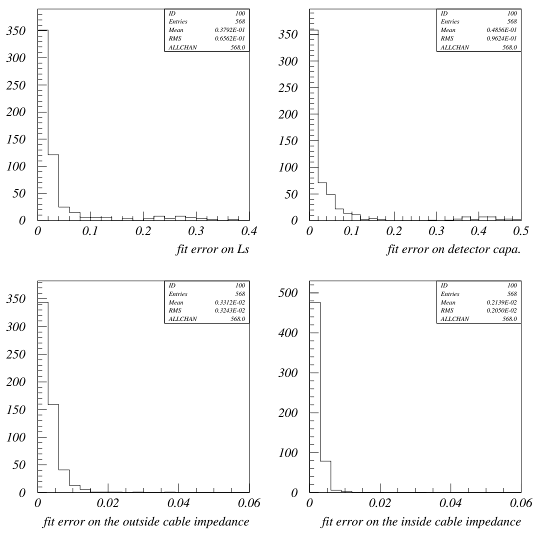

Figure 29: *Error distributions for the different parameters compute using channels measured several times*

T0-0	5	T1-0	0	T2-0	0	T3-0	0
T0-1	2	T1-1	1	T2-1	1	T3-1	0
T0-2	2	T1-2	1	T2-2	1	T3-2	0
T0-3	0	T1-3	2	T2-3	1	T3-3	0
T0-4	2	T1-4	2	T2-4	0	T3-4	0
T0-5	2	T1-5	1	T2-5	1	T3-5	1
T0-6	1	T1-6	0	T2-6	1	T3-6	1
T0-7	0	T1-7	1	T2-7	1	T3-7	1
T0-8	0	T1-8	1	T2-8	0	T3-8	0
T0-9	0	T1-9	0	T2-9	0	T3-9	1
T0-10	1	T1-10	1	T2-10	0	T3-10	1
T0-11	2	T1-11	1	T2-11	1	T3-11	1

Table 5: Number of channels measured 0,1,2,3,.. times each channel is measured on the reflectometry board. An addressing problem has mixed up several channels.

The error on the impedance determination procedure is small (0.34% for the outside cable and 0.21% for the inside cable. The error on L_s is also small (4%) but a little bump in the error distribution of L_s arround 25% should be noticed. This bump illustrates the fact that the fit on L_s is very sensitive to how well the peak of the strip signal is defined (zone 4 in figure 10). A change of one point in that region can drive the fit in a wrong direction. Moreover, there are very few points to perform the fit. The channels with a large error in this bump are, of course, cut off by the quality cuts. In a first approach we shall skip these channels in our calibration method. The correlation between the C_d fit and the L_s fit also emphasized before is shown by an other bump on the C_d with an error distribution around 40%. The channels corresponding to this bump are the same that the ones corresponding to the bump in L_s error distribution.

5.2 Final results

The same study has been performed on different preamplifiers species in the central region and in the endcaps. The final results on the accuracy of correction of the variation of the physics signal is given in table 9. In the encap region, two different families of parameters has been selected to obtained an error of 1.3% and 3% due to the net difference in cable lengths (fig 24. Tables 6 and 8 show that for those preamplifier types the large error value of table 9 is mostly given by the large values distribution of L_s and C_d. L_s is the strip inductance which drives the signal from the electrode to the cable. The L_s value is well correlated to the geometrical place of the channel in the calorimeter so in order to reduce the value distribution of L_s and also the error due to L_s, one can perform a calibration channel by channel but it is also possible to group type D ou C preamplifiers channels in η range (see figure 30). More than that C_d fitted values results are correlated to L_s fitted values because to perform C_d fits, L_s fitted values are injected as an input into the fitting function (see figure 31). Finally C_d should be correlated to η (see figure 32). The η range used to reduce L_s values distribution will also reduce C_d values distributions and reduce also the error due to C_d which is huge.

Theses results are obtained for calibration signals at the peak in time which is slightly different from one preamplifier specie to the other.

$\pm\sigma$ on :	$\delta(\Delta_{cal}^{t=t_{max}})$	$\delta(\Delta_{phys}^{t=t_{max}})$
$L_1 + L_2$	0.4%	0.02%
R_{c1} or R_{c2}	0.1%	0.4%
L_s	0.1%	0.9%
C_d	2.5%	2.1%

Table 6: Contributions in the errors on the variation of the calibration and physics signals from $\pm\sigma$ variations in the stable parameters distribution (type D preamp.)

$\pm\sigma$ on :	$\delta(\Delta_{cal}^{t=t_{max}})$	$\delta(\Delta_{phys}^{t=t_{max}})$
$L_1 + L_2$	0.3%	0.07%
R_{c1} or R_{c2}	0.3%	0.5%
L_s	0.01%	0.04%
C_d	1.1%	0.1%

Table 7: Contributions in the errors on the variation of the calibration and physics signals from $\pm\sigma$ variations in the stable parameters distribution (first group of type F preamp.)

$\pm\sigma$ on :	$\delta(\Delta_{cal}^{t=t_{max}})$	$\delta(\Delta_{phys}^{t=t_{max}})$
$L_1 + L_2$	0.4%	0.02%
R_{c1} or R_{c2}	0.2%	0.6%
L_s	0.3%	1.%
C_d	3.%	1.%

Table 8: Contributions in the errors on the variation of the calibration and physics signals from $\pm\sigma$ variations in the stable parameters distribution (first group of type C preamp.)

Preamp. species	$\delta(\Delta_{phys}^{t=t_{max}})$ each channel parameters	$\delta(\Delta_{phys}^{t=t_{max}})$ parameters mean values
E (central em.)	0.2%	0.4%
D (central had.)	0.2%	3.5%
F (endcap em.	0.1%	1.3%
C (endcap had.)	0.4%	3.5%

Table 9: Final errors on the variation of the physics signal when the parameters chosen correspond to the measured channel and when the mean values of the parameters is taken

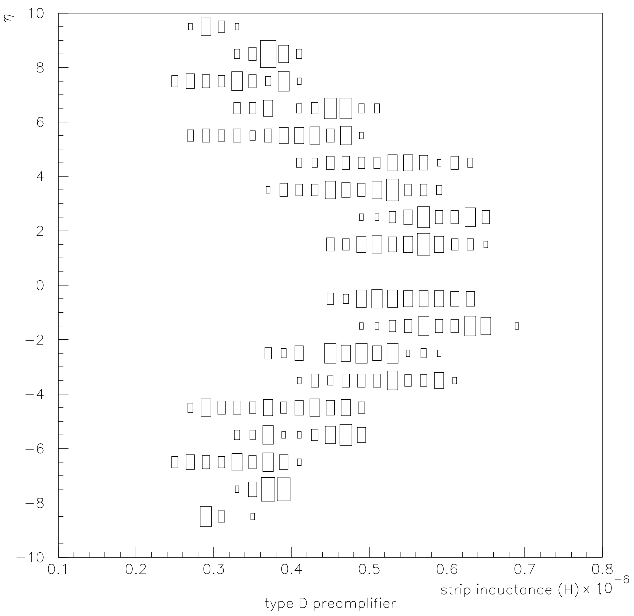

Figure 30: *fitted strip inductance values and η correlation for type D (central calorimeter) preamplifier*

6 Conclusion

In conclusion, from this study it seems feasible to perform a calibration of the calorimeter electronics much better than 1%, if we measure each channel parameters, over the whole calorimeter regions and a calibration of 3.5% if the channels are merged by preamplifier types. The same study as also been done for type H preamp., those preamplifiers are not as many as the other types described in this note but there are electromagnetic channels with large capacitance values so they give the worse results expected for an electromagnetic channel. The final error on the variation of the physics signal when the parameters chosen correspond to a measured channel is 0.4% and is 2.4% when the mean values of the parameters is taken.

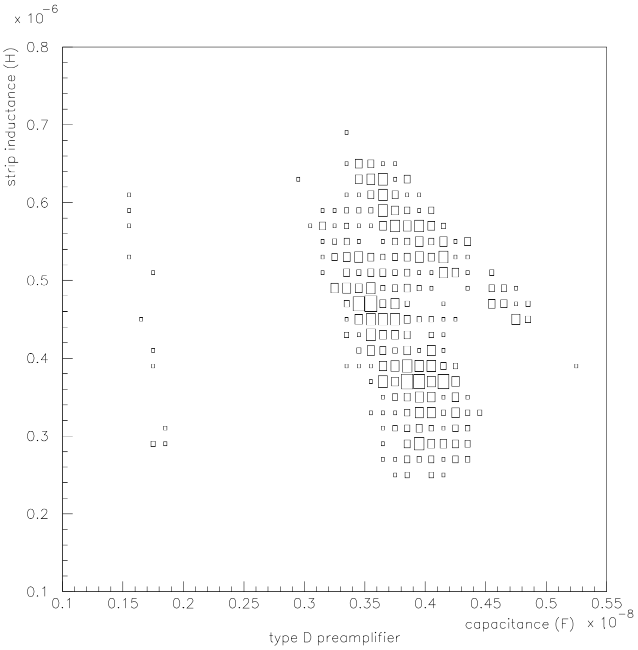

Figure 31: *fitted strip inductance and capacitance values correlation for type D (central calorimeter) preamplifier*

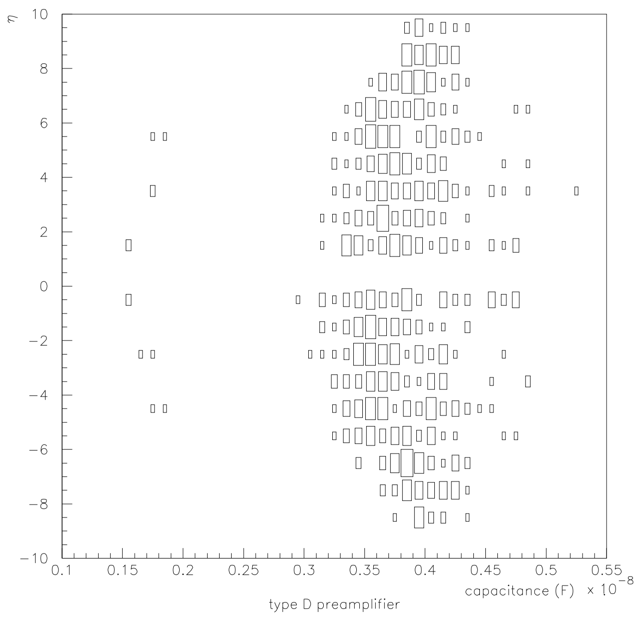

Figure 32: *fitted strip capacitance values and η correlation for type D (central calorimeter) preamplifier*

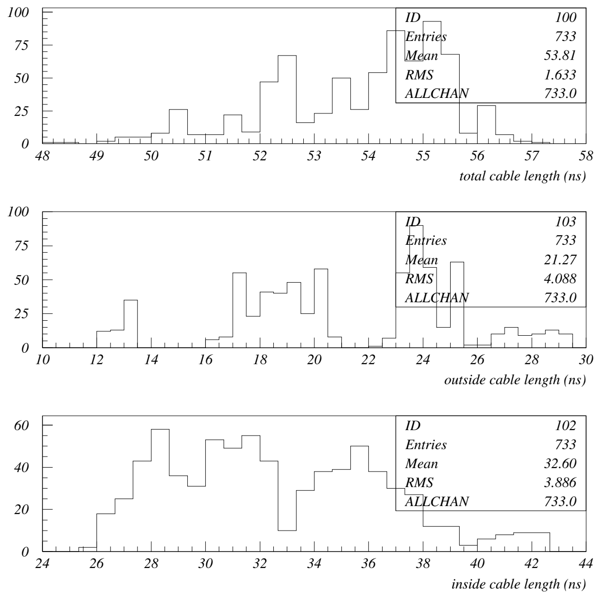

Figure 33: *cable length distributions for channels with type D preamp. (barrel)*

References

[1] Run II Calorimeter Calibration System P. Cornebise et al D0 note n0 3731

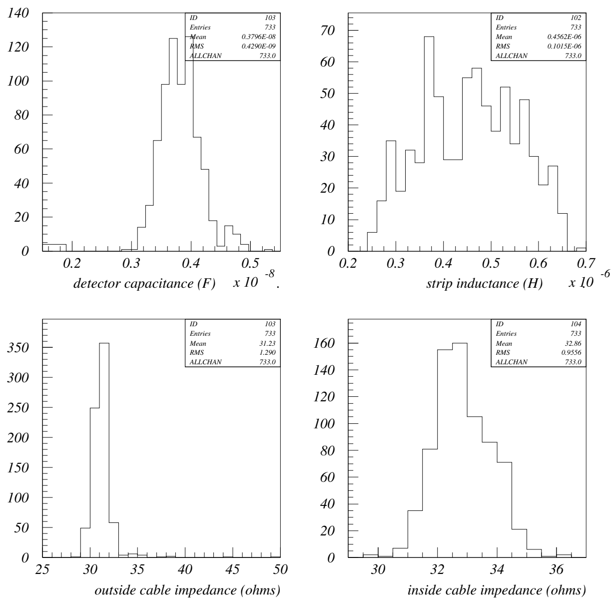

Figure 34: Rc_2, Rc_1, L_s *and* C_d *distributions for channels with type D preamp.*

7 Acknowledgments

The authors thank their colleagues from the LPNHE Paris for many fruitful discussions.

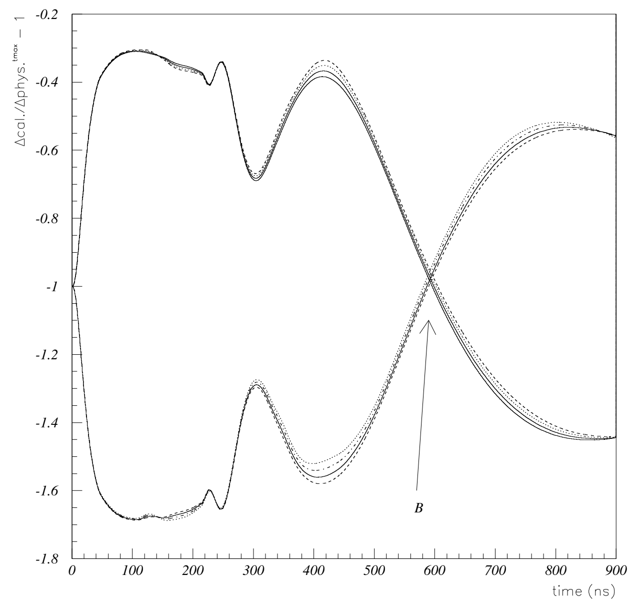

Figure 35: $\frac{\Delta cal^t}{\Delta phys^{t_{max}}} - 1$ *for a variation of* Z_{in} *of* $\pm 5\%$, $\pm 10\%$, $\pm 15\%$ *and* $\pm 20\%$ *(type D preamp.)*

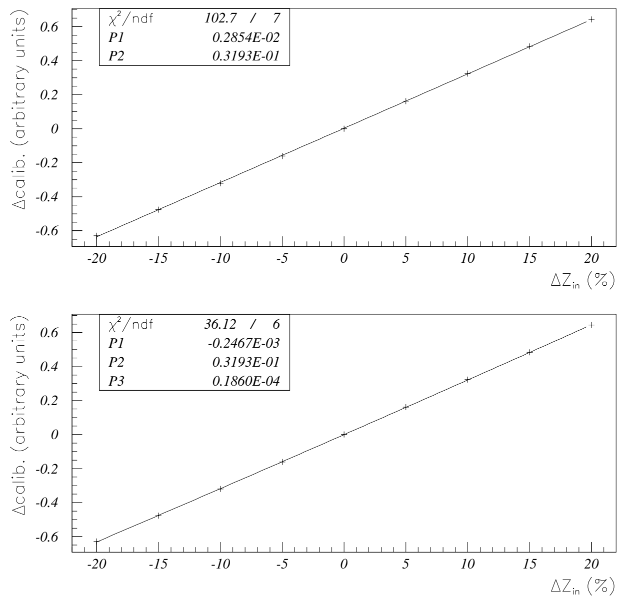

Figure 36: *linear fit (on top) and polynomial fit (on bottom) results of* $\Delta cal(t = peak\ in\ time$*, calibration peak in time for standard parameter set) as a function of* $\Delta Z_{in}(in\%)$ *(type D preamp.)*

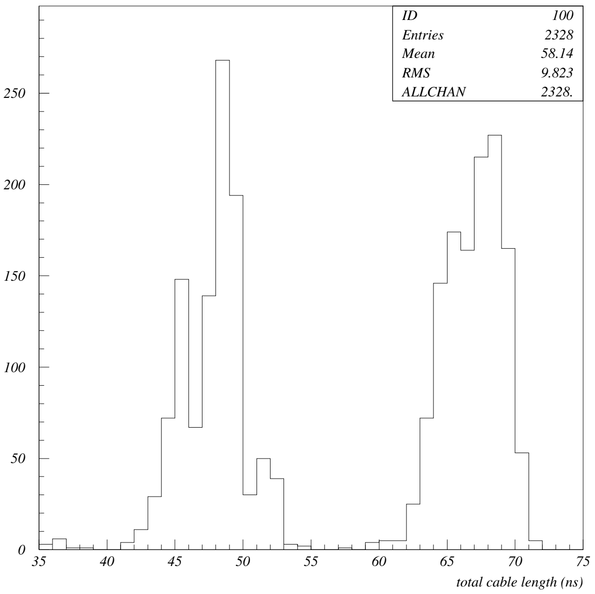

Figure 37: *cable length distributions for channels with type F preamp. (end cap). Serapation of type F channels into 2 groups is needed.*

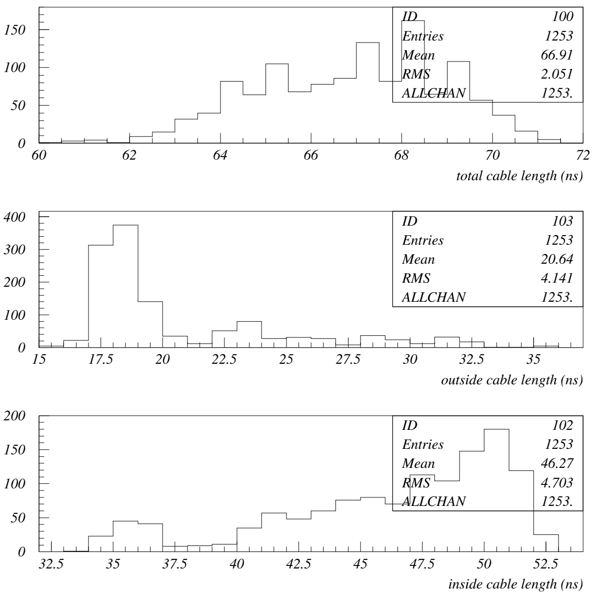

Figure 38: *cable length distributions for channels with type F preamp. for one group (end cap)*

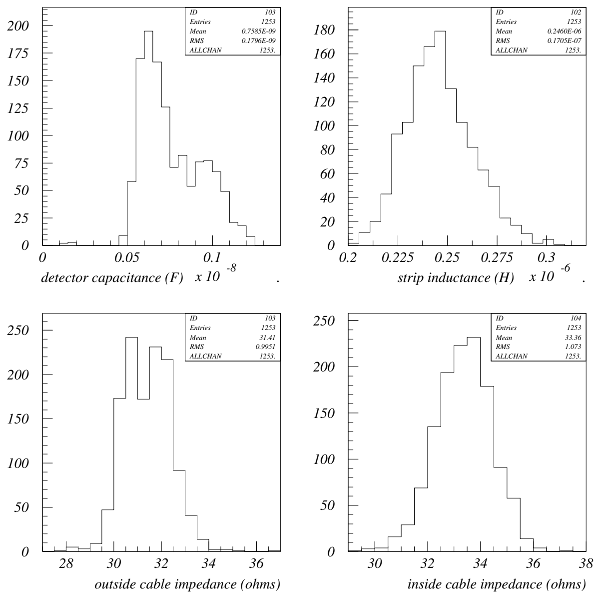

Figure 39: *Rc_2, Rc_1, L_s and C_d distributions for channels with type F preamp.*

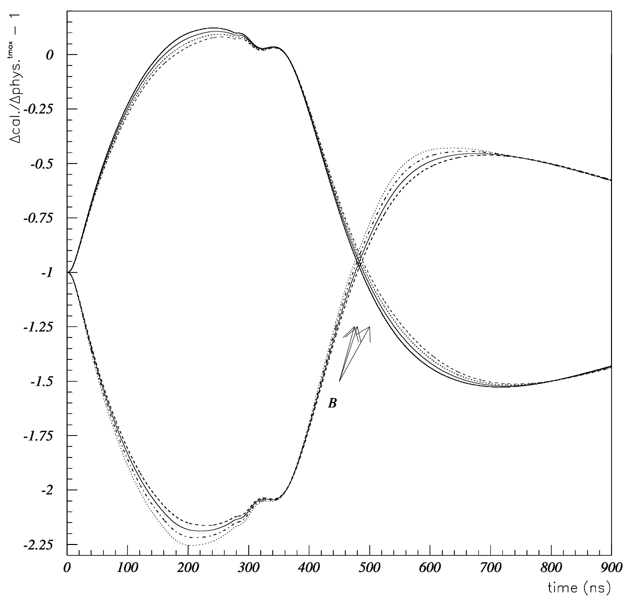

Figure 40: $\frac{\Delta cal^t}{\Delta phys^{t_{max}}} - 1$ *for a variation of* Z_{in} *of* ±5%, ±10%, ±15% *and* ±20% *(type F preamp.)*

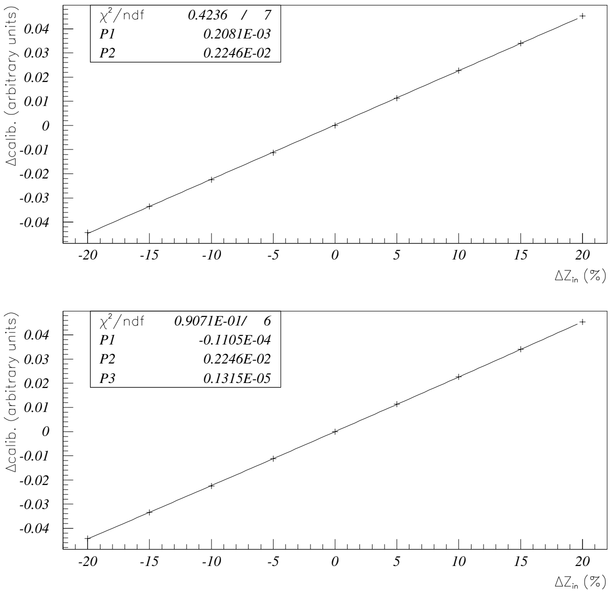

Figure 41: *linear fit (on top) and polynomial fit (on bottom) results of* $\Delta cal(t = peak\ in\ time,$ *calibration peak in time for standard parameter set) as a function of* $\Delta Z_{in}(in\%)$ *(type F preamp.)*

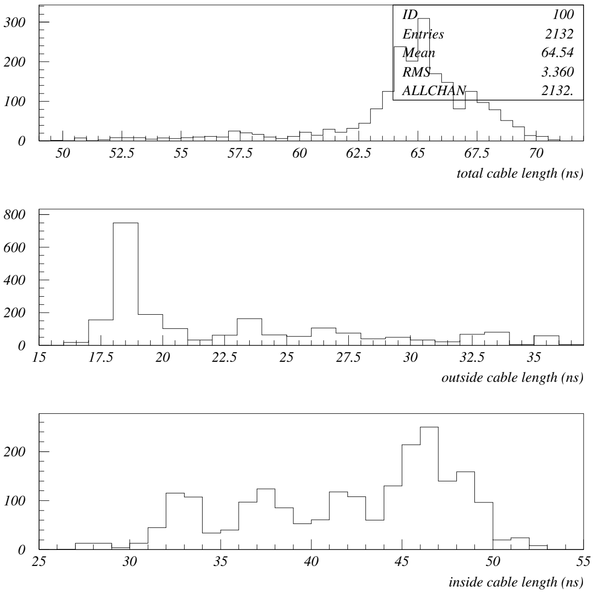

Figure 42: *cable length distributions for channels with type C preamp. for one group (end cap)*

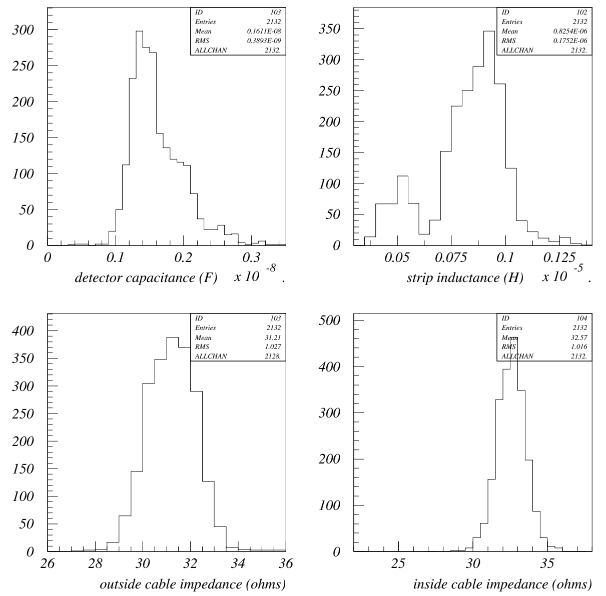

Figure 43: Rc_2, Rc_1, L_s *and* C_d *distributions for channels with type C preamp.*

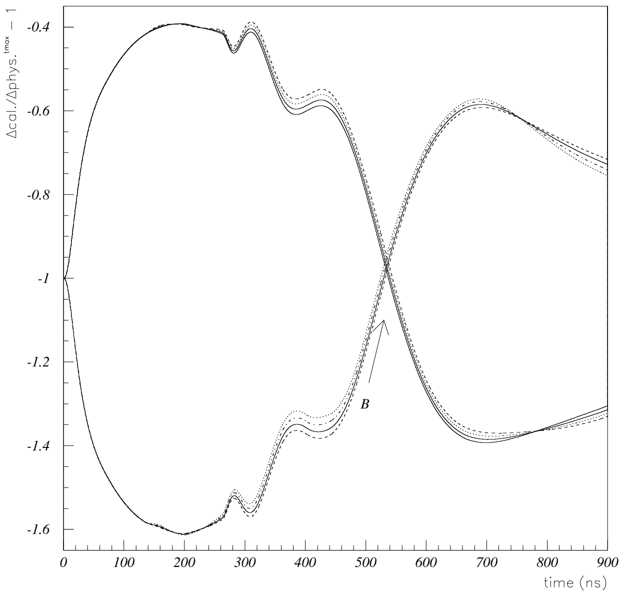

Figure 44: $\frac{\Delta cal^t}{\Delta phys^{t_{max}}} - 1$ *for a variation of* Z_{in} *of* $\pm 5\%$, $\pm 10\%$, $\pm 15\%$ *and* $\pm 20\%$ *(type C preamp.)*

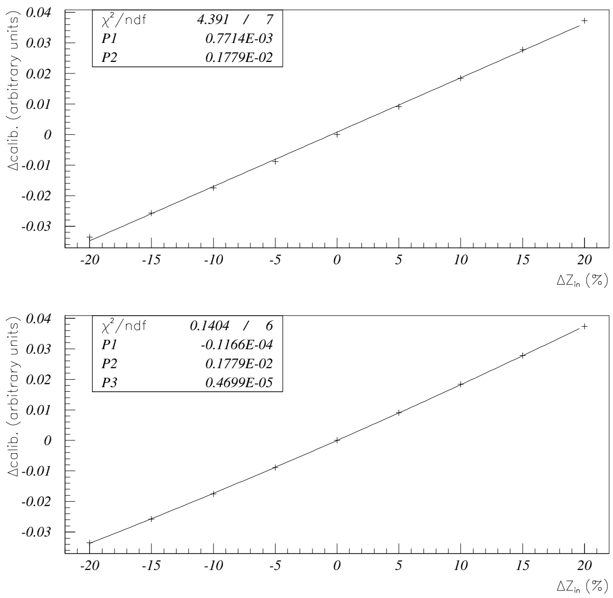

Figure 45: *linear fit (on top) and polynomial fit (on bottom) results of* $\Delta cal(t =$ *peak in time, calibration peak in time for standard parameter set) as a function of* $\Delta Z_{in}(in\%)$ *(type C preamp.)*

A Annex : Modelization and Simulation of Physics and Calibration for D0 experiment.

We know that the Physics and Calibration signals do not follow the same path and have to be modelized separately.

In order to be able to make a simulation of this scheme, four procedures have been applied :

- The first one is a modelization of the transfer functions for the Physics and Calibration parts until the input impedance of the preamplifier Z0 using the well known Laplace-Transform method. The same thing has been applied upon the Preamplifier Transfer Function (TF).
- The second one is application of the Skin Effect TF on cable response.
- The third one is the transformation of these Laplace TF into equations which can be directly simulated with any language like C or Fortran : it is the Z-Transform which gives the possibility to obtain signals in time domain.
- The fourth one is the convolution of the results for each part with a measured impulse function of the Shaper (no correct model is available).

After all these procedures we are able to reach our goal which was to have the signal at the Shaper output in time domain.

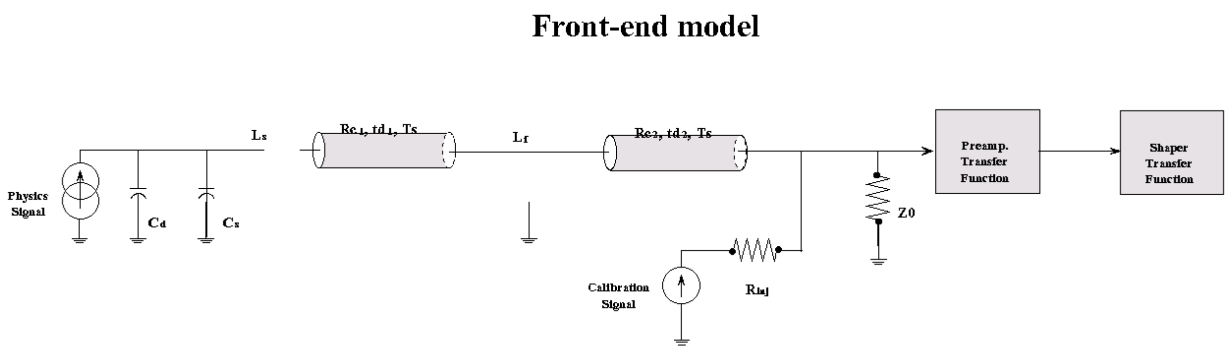

Figure 46:

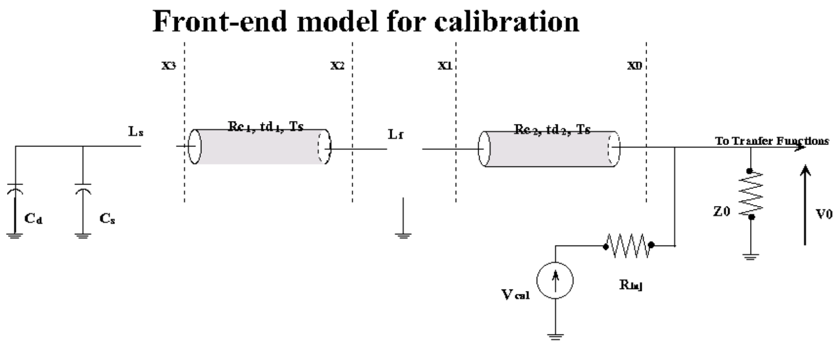

Figure 47:

A.1 Laplace domain modelizations :

A.1.1 Calibration modelization before Preamplifier :

Using Laplace domain transform, the goal is to find the $V_0(s)$ function vs Vcal(s).

$$V_0(s) = \frac{(Z_0//X_0(s))}{(Z_0//X_0(s))+Rinj}.Vcal(s)$$

- Z_0 is the input impedance of the Preamplifier. It is supposed to be a pure resistive component.

It is possible to compute real Preamplifier input impedance but in the frequency domain of our interest, it is close to a simple resistor.

- Rinj is the injection output resistor. As for Z_0, the real injection impedance is not really a resistor but is very close from it.
- Xi(s) (i from 0 to 3) is the equivalent impedance of the left part of the scheme. It can be explained in function of model parameters.

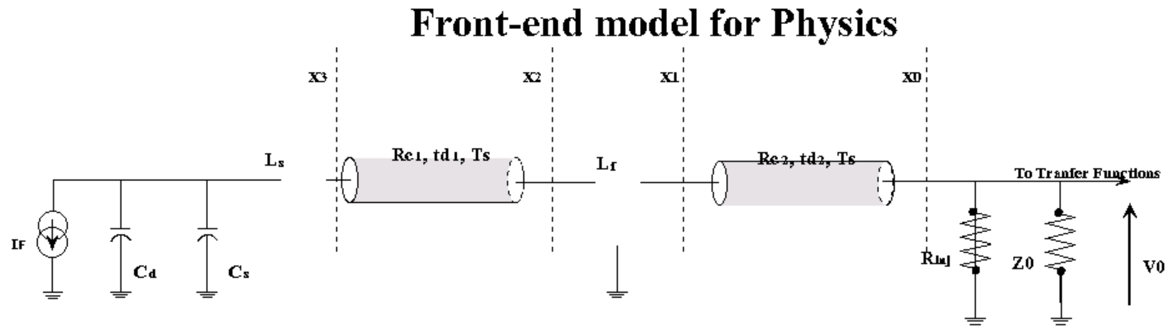

Figure 48:

- Vcal(s) is the calibration voltage generator which Laplace function is computed upon the switch model already described.

$$X_0(s) = Rc_2.\frac{1+\Gamma_{L2}(s).e^{-2td_2 s}}{1-\Gamma_{L2}(s).e^{-2td_2 s}} \qquad \Gamma_{L2}(s) = \frac{X_1(s)-Rc_2}{X_1(s)+Rc_2}$$

$$X_1(s) = L_f s + X_2(s)$$

$$X_2(s) = Rc_1.\frac{1+\Gamma_{L1}(s).e^{-2td_1 s}}{1-\Gamma_{L1}(s).e^{-2td_1 s}} \qquad \Gamma_{L1}(s) = \frac{X_3(s)-Rc_1}{X_3(s)+Rc_1}$$

$$X_3(s) = L_s s + \frac{1}{C_T s} \qquad C_T = C_d + C_s$$

A.1.2 Physics modelization before Preamplifier :

Using Laplace domain transform, the goal is to find the $V_0(s)$ function vs $I_\Phi(s)$.

$$V_0(s) = \frac{[1+\Gamma_{L2}].e^{-td_2 s}}{1+\Gamma_{L2}.e^{-2td_2 s}}.V_1(s)$$

- Xi(s) (i from 0 to 3) is the equivalent impedance from point Xi to all the right part of the scheme.
- Vi(s) (i from 0 to 3) is the voltage measurement at point Xi.
- $I_\Phi(s)$ is the Physics current generator which function is computed upon well known model.
- $I_L(s)$ is the current inside in L_S inductance.

$$V_1(s) = \frac{X_1(s)}{L_f\ s+X_1(s)}.V_2(s) \qquad \Gamma_{L2} = \frac{X_0-Rc_2}{X_0+Rc_2}$$

$$X_0 = Rinj\ //\ Z_0 \qquad X_1(s) = Rc_2.\frac{1+\Gamma_{L2}.e^{-2td_2 s}}{1-\Gamma_{L2}.e^{-2td_2 s}}$$

$$V_2(s) = \frac{[1+\Gamma_{L1}(s)].e^{-2td_1 s}}{1-\Gamma_{L1}(s).e^{-2td_1 s}}.V_3(s) \qquad \Gamma_{L1}(s) = \frac{X_2(s)-Rc_1}{X_2(s)+Rc_1}$$

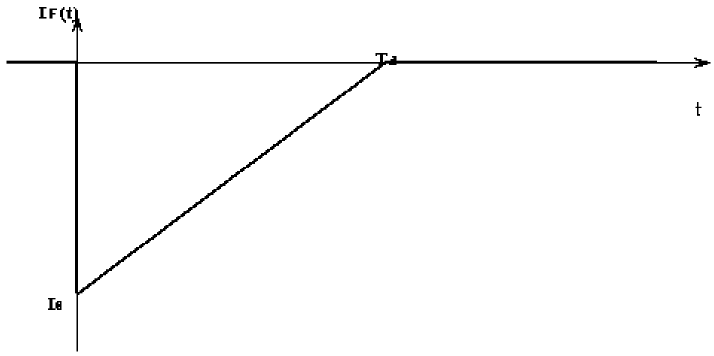

Figure 49:

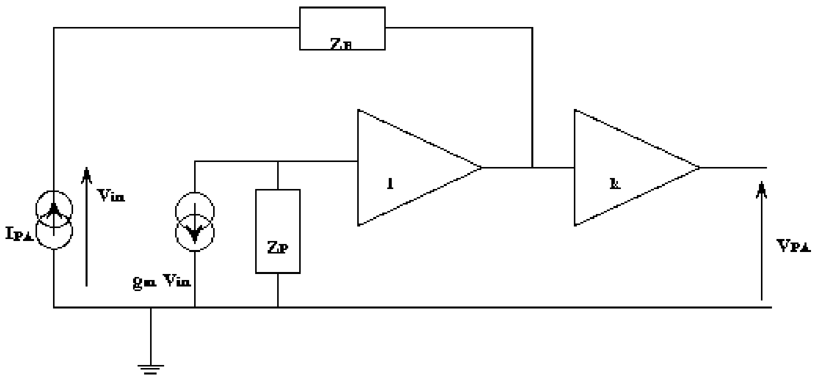

Figure 50:

$X_2(s) = L_f\ s + X_1(s)$ $\qquad$ $X_3(s) = Rc_1 . \frac{1+\Gamma_{L1}(s).e^{-2td_1 s}}{1-\Gamma_{L1}(s).e^{-2td_1 s}}$

$V_3(s) = X_3(s).I_L(s)$ $\qquad$ $I_L(s) = \frac{\frac{1}{C_T\ s}}{\frac{1}{C_T\ s}+L_s\ s+X_3(s)}\ I_\Phi(s).$

A.1.3 Physics pulse model :

The well known physics pulse shape is drawn below :

$$i_\Phi(t) = I_0 . \left(1 - \frac{t}{T_d}\right)(h_v(t) - h_v(t - T_d))$$
$$I_\Phi(s) = \pounds\left[i_\Phi(t)\right](s) = I_0 \frac{T_d\, s - 1 + e^{-T_d\, s}}{T_d\, s^2}$$

A.1.4 Preamplifier model :

$Z_0(s) = \frac{Z_f(s)}{1+gm\, Z_P(s)}$ $\qquad$ $Z_f(s) = r_f \ // \ (r_{f1} + \frac{1}{C_f\ s})$ $\qquad$ $Z_P(s) = R_P \ // \ (r_P + \frac{1}{C_P\ s})$

$$V_{PA}(s) = -k\ gm\ Z_P(s)\, V_0(s) = -k\ gm\ Z_P(s)\ Z_0(s)\ I_{PA}(s)$$

A.2 Skin Effect :

The Skin Effect is the result of the magnetic field inside the conductor at high frequencies. It "pushes" the electrons to the borders of the central conductor of the cable depending on their frequency.

The result of this physics phenomenon is an equivalent resistor :

$$R_{SKIN}(s) = \frac{J_0(\sqrt{\mu\ \sigma\ s}R)\ \sqrt{\mu\ \sigma\ s}}{J_1(\sqrt{\mu\ \sigma\ s}R)\ 2\pi R\,\sigma}$$

J are Bessel functions, μ the permeability, σ the conductivity, R the radius of the conductor.

This complex function may be approximated at high frequencies by a simpler form :

$$R_{SKIN}(s) = K\sqrt{s}$$

Then the cable response modification due to the Skin Effect may be calculated. The principal change is in the propagation function :

$$\gamma(s) = \sqrt{(R + Ls)(G + Cs)} = \sqrt{(K\sqrt{s} + Ls)\ Cs} \text{ for lossless cables.}$$

The at the first order :

$$\gamma(s)l = \tau s + \frac{K\,l\sqrt{s}}{2\,Rc}$$

The first term is a pure delay and pulse response of the second term can be calculated :

$$h_{SKIN}(t) = \pounds^{-1}\left[e^{-\frac{K\,l\sqrt{s}}{2\,Rc}}\right](t) = \frac{1}{T_S\pi}\left(\frac{T_S}{t}\right)^{\frac{3}{2}} e^{-\frac{T_s}{t}} \qquad Ts = \left(\frac{K\ l}{4\ Rc}\right)^2$$

A.3 Digital Filtering :

The goal is to translate all Laplace functions into digital filtering. The Z-transform is used to compute TF application in time domain for two main reasons : one knows a bilinear equivalence between s and Z variables and delay are easy to simulate :

$$s \approx \frac{2}{T}\frac{1-Z}{1+Z} \qquad e^{-T\,s} = Z \qquad Z\ e(t) = e(t-T)$$

Choosing the sampling period T to be short enough in comparison with all time constants and delay in TF allows to do not make modelization error at frequencies two times below the sampling frequency. In all cases, the Z TF will be a polynomial rational function :

$$H(s) = e^{-kTs}\frac{\sum A_i\ s^i}{\sum B_j\ s^j} \Rightarrow H(Z) = Z^k\ \frac{\sum a_i\ Z^i}{\sum b_j\ Z^j}$$

A time representation of a signal e will give a signal s transformed by the H TF :

$$e(t) \rightarrow H \rightarrow s(t)$$

At sampling time : t=nT

$$e_n \rightarrow H \rightarrow s_n \qquad s_n = H(Z)\ e_n = Z^k\ \frac{\sum a_i\ Z^i}{\sum b_j\ Z^j}\,e_n$$

$$\sum b_j\ Z^j\ s_n = Z^k\ \sum a_i\ Z^i\ e_n \qquad \sum b_j\ s_{n-j} = \sum a_i\ e_{n-i-k}$$

$$\boxed{s_n = \frac{\sum_{i=0}^{N} a_i\ e_{n-i-k} - \sum_{j=1}^{M} b_j\ s_{n-j}}{b_0}}$$

N and M are the samples number for e and s respectively.

Using this method, one can easily compute all signal values at sampling time.

A.4 Digital Convolution :

When it is not possible to obtain the Laplace form of a TF (for the Shaper) or when this form is not a polynomial function (for the Skin Effect), it is possible to use the convolution with the impulse time-domain function h(t) :

$$s(t) = (h * e)\,(t) = \int_{-\infty}^{+\infty} h(t-u)\ e(u)\ du$$
$$s(nT) = \int_{-\infty}^{+\infty} h(nT-u)\ e(u)\ du = \sum_{k=-\infty}^{+\infty}\ \int_{kT}^{(k+1)T} h(nT-u)\ e(u)\ du$$

Supposing T is chosen to be small enough in comparison with h and e variations, it can be assumed that h and e are constant inside a T interval :

$$s(nT) = \sum_{k=-\infty}^{+\infty} T\ h(nT-kT)\ e(kT) \Rightarrow \boxed{s_n = T\ \sum_k h_{n-k}\ e_k}$$